

ARTICLE

N-glycanase NGLY1 regulates mitochondrial homeostasis and inflammation through NRF1

Kun Yang^{1,2} , Ryan Huang^{1,2}, Haruhiko Fujihira^{3,4}, Tadashi Suzuki³, and Nan Yan^{1,2} 

Mutations in the *NGLY1* (N-glycanase 1) gene, encoding an evolutionarily conserved deglycosylation enzyme, are associated with a rare congenital disorder leading to global developmental delay and neurological abnormalities. The molecular mechanism of the *NGLY1* disease and its function in tissue and immune homeostasis remain unknown. Here, we find that *NGLY1*-deficient human and mouse cells chronically activate cytosolic nucleic acid-sensing pathways, leading to elevated interferon gene signature. We also find that cellular clearance of damaged mitochondria by mitophagy is impaired in the absence of *NGLY1*, resulting in severely fragmented mitochondria and activation of cGAS-STING as well as MDA5-MAVS pathways. Furthermore, we show that *NGLY1* regulates mitochondrial homeostasis through transcriptional factor NRF1. Remarkably, pharmacological activation of a homologous but nonglycosylated transcriptional factor NRF2 restores mitochondrial homeostasis and suppresses immune gene activation in *NGLY1*-deficient cells. Together, our findings reveal novel functions of the *NGLY1*-NRF1 pathway in mitochondrial homeostasis and inflammation and uncover an unexpected therapeutic strategy using pharmacological activators of NRF2 for treating mitochondrial and immune dysregulation.

Introduction

The N-glycanase 1 (*NGLY1*), also known as peptide:N-glycanase (PNGase), is an evolutionarily conserved enzyme that removes N-glycans from glycosylated proteins in the cytosol (Suzuki et al., 2016). *NGLY1* plays a crucial role in quality control for newly synthesized N-glycoproteins. For example, during ER-associated degradation, misfolded N-glycoproteins are retrotranslocated from the ER lumen to the cytosol (Hirsch et al., 2003). *NGLY1* removes N-glycans from these misfolded proteins before they can be degraded by the proteasome. Mutations in the *NGLY1* gene are associated with a rare congenital disorder affecting mostly young children (IMIM 615273 and 610661; Enns et al., 2014; Lam et al., 2017). Almost all *NGLY1* missense and nonsense mutations reduce the *NGLY1* protein level and enzymatic activity (He et al., 2015). Clinical features of *NGLY1*-deficient patients include global developmental delay, neurological disorders, and liver disease (Enns et al., 2014), clearly indicating the physiological importance of the enzyme.

One important substrate of *NGLY1* is the ER-associated glycosylated transcription factor nuclear factor, erythroid 2 like 1 (*Nfe2l1*, also known as *Nrf1*). *Nrf1* requires deglycosylation by *NGLY1* and proteolysis by DNA Damage Inducible 1 Homologue 2 (*DDI2*) before nuclear translocation, where the nuclear form of *Nrf1* drives expression of proteasome subunit genes (Tomlin

et al., 2017; Owings et al., 2018). *Nrf1* plays an important role in the proteasome “bounce-back” mechanism where it drives expression of proteasome subunit genes in response to proteotoxic stress (Radhakrishnan et al., 2010). Interestingly, *Nrf2*, a close homologue of *Nrf1*, is not glycosylated, responds to oxidative stress, and regulates similar proteasome subunit genes, as does *Nrf1* (Kwak et al., 2003). *Nrf2* also regulates expression of autophagy and mitophagy genes (East et al., 2014; Pajares et al., 2016).

Despite severe developmental and neurological disabilities in *NGLY1* children, interestingly, parents often report that these affected *NGLY1* children “oddly” appear to be resistant to common childhood viral infections (Mnookin, 2014). Similar viral resistance phenotypes were also reported in patients with chronically activated type I IFN response that are caused by mutations in nucleic acid metabolizing enzymes such as *TREX1* and *RNaseH2* (Hasan et al., 2013; Pokatayev et al., 2016). *TREX1* and *RNaseH2* mutations were associated with a neuro-inflammatory disease called Aicardi-Goutières syndrome (AGS). We and others have shown that *TREX1*- and *RNaseH2*-associated AGS is caused by accumulation of self-DNA in the cytosol and activation of the innate immune DNA-sensing pathway (Crow and Manel, 2015). Innate immune detection of microbial or self-DNA by the DNA sensor cGAS activates downstream STING-TBK1-IRF3 signaling

¹Department of Immunology, University of Texas Southwestern Medical Center, Dallas, TX; ²Department of Microbiology, University of Texas Southwestern Medical Center, Dallas, TX; ³Glycometabolic Biochemistry Laboratory, Institute of Physical and Chemical Research (RIKEN) Cluster for Pioneering Research, Saitama, Japan; ⁴Division of Glycobiology, Intractable Disease Research Center, Juntendo University Graduate School of Medicine, Tokyo, Japan.

Correspondence to Nan Yan: nan.yan@utsouthwestern.edu.

© 2018 Yang et al. This article is distributed under the terms of an Attribution-Noncommercial-Share Alike-No Mirror Sites license for the first six months after the publication date (see <http://www.rupress.org/terms/>). After six months it is available under a Creative Commons License (Attribution-Noncommercial-Share Alike 4.0 International license, as described at <https://creativecommons.org/licenses/by-nc-sa/4.0/>).

cascade, leading to type I IFN and inflammatory responses and induction of IFN-stimulated genes (ISGs) that resembles an antiviral state (Wu and Chen, 2014). A parallel cytosolic RNA-sensing pathway begins with RIG-I or MDA5 recognizing the RNA ligand, then signals through MAVS-TBK1-IRF3 to activate IFN response. Gain-of-function mutations in MDA5 are also associated with AGS (Crow and Manel, 2015). Mitochondrial and nuclear genomic DNA are major sources of self-DNA, which can accumulate in the cytosol during mitochondrial stress (West et al., 2015), DNA damage (Härtlova et al., 2015), or deficiency in cytosolic nucleic acid metabolizing enzymes, such as TREX1 (Stetson et al., 2008; Wolf et al., 2016), and cause a broad range of autoimmune and inflammatory diseases, including AGS and systemic lupus erythematosus (SLE; Yan, 2017). In this study, we report novel innate immune and mitochondrial defects associated with *NGLY1* deficiency. We also present the underlying molecular mechanism of these defects and an unexpected therapeutic strategy for treating *NGLY1* patients.

Results

Increased expressions of ISGs in *Ngly1*-deficient cells

We first investigated whether *Ngly1* deficiency is associated with increased expression of ISGs, also known as the IFN gene signature, that is commonly observed in autoimmune diseases such as type I interferonopathy and cells at an antiviral state (Hasan et al., 2013; Pokatayev et al., 2016). We found that several ISGs were up-regulated in *Ngly1*^{-/-} murine embryonic fibroblasts (MEFs), compared with littermate WT cells (Fig. 1, A and B). We also knocked down *Ngly1* expression using shRNA and observed increased ISG expression in two independent lines of *Ngly1* shRNA-expressing cells (Fig. 1, C and D). To further determine whether the increased ISG expression is caused by the lack of *Ngly1* enzymatic activity, we stably expressed WT or an enzymatically inactive *Ngly1* mutant C306A (Hirsch et al., 2003) in *Ngly1*^{-/-} MEFs using a retroviral vector (Fig. 1, E and F). WT *Ngly1* expression in *Ngly1*^{-/-} MEFs significantly reduced ISG expression down to close to normal levels, but *Ngly1* mutant C306A did not (Fig. 1, E and F), demonstrating that the N-glycanase activity is critical for inhibiting ISG expression. We previously showed that cell-intrinsic activation of ISGs renders cells to become resistant to viral infections (Hasan et al., 2013; Pokatayev et al., 2016). We challenged WT and *Ngly1*^{-/-} MEFs with vesicular stomatitis virus (VSV), and we found that VSV replication was significantly inhibited in *Ngly1*^{-/-} MEFs, consistent with an overall antiviral state (Fig. 1 G).

To determine whether *NGLY1* deficiency also cause innate immune activation in human cells, we generated *NGLY1* knockout THP-1 cells (a human monocytic cell line) using CRISPR/Cas9 (Fig. 1 H). Three independent clones of *NGLY1*^{KO} THP-1 cells all showed robustly increased ISG expression compared with WT and two nontargeting control cell lines (Fig. 1 H). We next examined lymphoblastoid cell lines from *NGLY1* patients and four healthy controls. *NGLY1* patient cells show reduced or undetectable *NGLY1* protein and elevated expression of several ISG transcripts compared with healthy controls (Fig. 1 I). Collectively, our data showed that *NGLY1* deficiency in both human and mouse

cells activate innate immune signaling leading to increased expression of ISGs that resemble an antiviral state.

Innate immune nucleic acid-sensing pathways are activated in *NGLY1*-deficient cells

We next sought to determine which innate immune signaling pathway is involved in inducing ISG expression in *NGLY1*-deficient cells. We first used inhibitors that block key kinases required for innate immune signaling. TBK1 inhibitors (Compound II [Hasan et al., 2015] and BX-795) and IKK-ε inhibitor (CAY10576) completely suppressed ISG expression in *Ngly1*^{-/-} MEFs, while IKK-α/β inhibitor (BAY11-7082) partially decreased ISGs expression (Fig. 2 A). We next used siRNAs to knockdown key components of the cytosolic DNA- (via cGAS-STING-TBK1-IRF3) and RNA- (via RIG-I/MDA5-MAVS-TBK1-IRF3) sensing pathways (Fig. 2 B). We found that knockdown of *cGas*, *Sting*, or *Irf3* completely abolished the elevated ISG expression in *Ngly1*^{-/-} MEFs (Fig. 2 C). Knockdown of *MDA5* or *Mavs*, which are required for sensing cytosolic RNA, also reduced overall ISG expression, although residual ISG expression in *Ngly1*^{-/-} MEFs remained higher than WT controls, suggesting that RNA-sensing pathways are partially required for innate immune activation in *Ngly1*^{-/-} MEFs (Fig. 2 D). We next generated shRNA-mediated stable knockdown of *Sting* or *cGas*, and both completely suppressed ISG expression in *Ngly1*^{-/-} cells (Fig. 2 E). We further measured phosphorylation of STING (Ser365) and found increased phospho-STING in *Ngly1*^{-/-} cells compared with littermate *Ngly1*^{+/+} cells (in which low baseline phosphorylation was detected), providing direct evidence for the activation of the cGAS-STING pathway (Fig. S1).

Ngly1^{-/-} mice are reported to be embryonic lethal (on the C57BL/6 background; Fujihira et al., 2017). We next bred *Ngly1*^{-/-} mice to *Sting*^{-/-}, *Mavs*^{-/-} or *Ifnar*^{-/-} mice to test whether ablation of either cytosolic DNA or RNA sensing or type I IFN signaling pathway could eliminate innate immune activation and rescue embryonic lethality of *Ngly1*^{-/-} mice. We found that all double knockout neonates were still-born or died soon after birth, similar to *Ngly1*^{-/-} alone (Fig. 2 F; Table 1). We then isolated primary MEFs from each double knockout embryos at day E13.5 and found that *Ngly1*^{-/-}*Sting*^{-/-} completely suppressed ISGs expression to the low levels of *Ngly1*^{+/+}*Sting*^{-/-}, whereas *Ngly1*^{-/-}*Mavs*^{-/-} MEFs showed substantial but incomplete suppression of ISGs (Fig. 2, G and H), consistent with the RNAi knockdown data. Together, these data suggest that *NGLY1* deficiency leads to aberrant activation of cytosolic nucleic acid-sensing pathways, especially the cGAS-STING pathway. The genetic evidence also suggests that innate immune activation is unlikely to be the main cause of embryonic lethality of *Ngly1*^{-/-}, thus the process upstream of immune activation needs to be explored.

NGLY1-deficient cells exhibit fragmented mitochondria and aberrant mtDNA release into the cytosol

We next explored the cause of immune activation and potential molecular pathogenesis of *Ngly1* deficiency. Nuclear genomic and mitochondrial DNA (mtDNA) are major sources of endogenous ligand for the cGAS-STING DNA-sensing pathway (Rongvaux et al., 2014; White et al., 2014; Härtlova et al., 2015). Since cGAS is the main cytosolic DNA sensor and is required for ISG induction

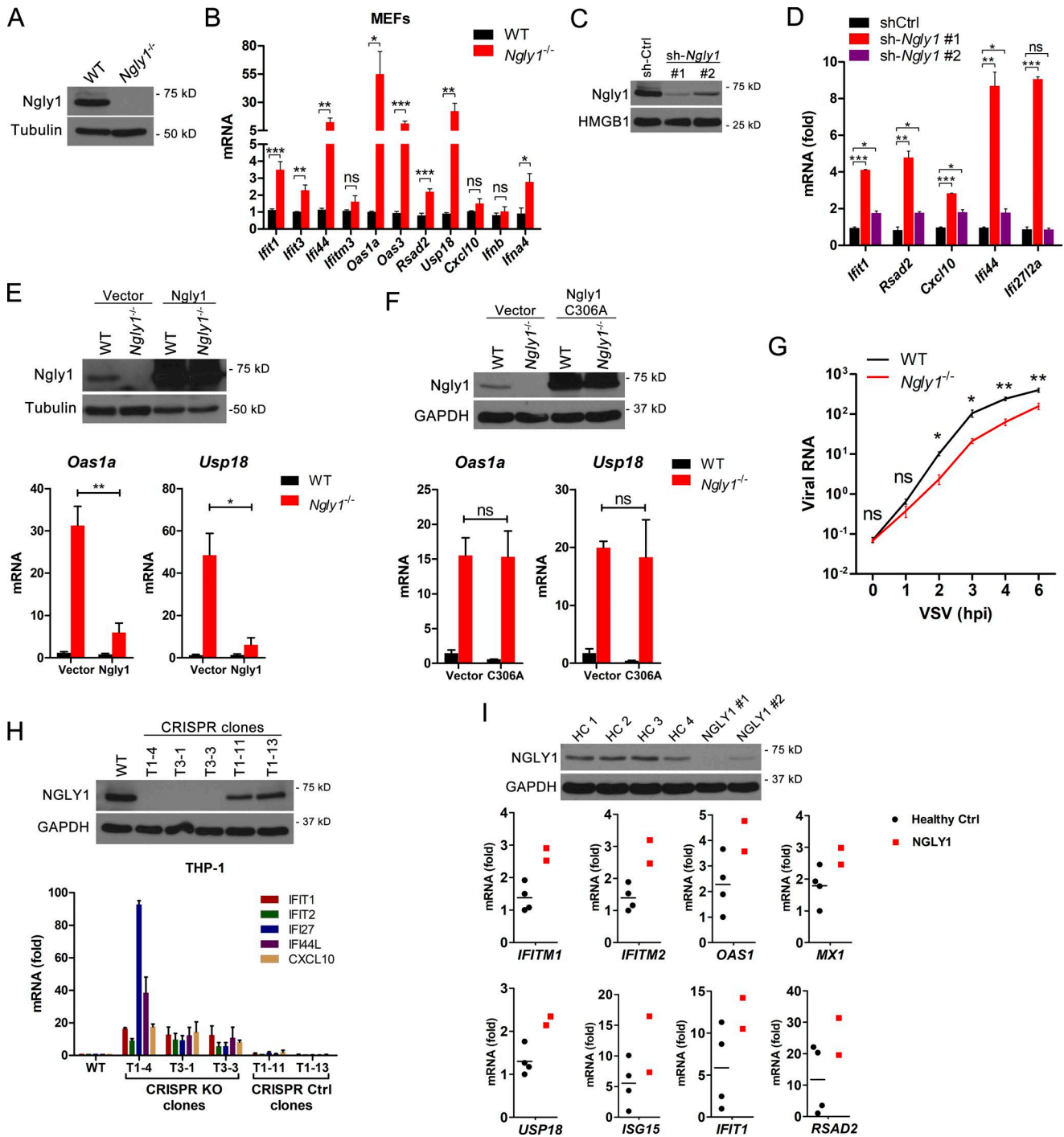


Figure 1. **NGLY1**-deficient cells show increased expression in ISGs. **(A)** Western blot analysis of Ngly1 in WT and *Ngly1*^{-/-} MEFs. Tubulin was used as a loading control. **(B)** PCR array of ISGs expression in WT and *Ngly1*^{-/-} MEFs. Gene expression was normalized to the housekeeping gene *Gapdh* (same throughout). Data are representative of at least three independent experiments. Unpaired Student's *t* test. **(C)** Western blot analysis of Ngly1 in MEFs transduced with indicated shRNA lentiviruses. **(D)** Quantitative RT-PCR analysis of ISGs in MEFs transduced with indicated shRNA lentivirus. Data are representative of at least two independent experiments. **(E and F)** Western blot analysis (upper panels) of Ngly1 in WT and *Ngly1*^{-/-} MEFs retrovirally transduced with WT or enzymatically inactive C306A mutant Ngly1. Quantitative RT-PCR analysis of ISGs (lower panels) in WT and *Ngly1*^{-/-} MEFs transduced with indicated Ngly1. Data are representative of at least three independent experiments. Student's *t* test. **(G)** Quantitative RT-PCR analysis of VSV viral RNA in WT and *Ngly1*^{-/-} MEFs infected with VSV for indicated time. Viral RNA level was calculated as compared with the housekeeping gene *Gapdh*. Student's *t* test. **(H)** Western blot analysis of NGLY1 (upper panel) and quantitative RT-PCR analysis of ISGs (lower panel) in WT and NGLY1-CRISPR knockout THP-1 clones. Gene expression was normalized to the housekeeping gene *GAPDH*. Error bars, SEM. Data are representative of at least three independent experiments. **(I)** Western blot of NGLY1 (upper panel) and quantitative RT-PCR analysis of ISGs (lower panel) in healthy controls (*n* = 4) and NGLY1 patients (*n* = 2). Gene expression was normalized to the housekeeping gene *GAPDH*. ISG expression of one healthy control was arbitrarily set as 1 and fold change of gene expression was calculated in other individuals. *, *P* < 0.05; **, *P* < 0.01; ***, *P* < 0.001; ns indicates not significant. Error bars, SEM.

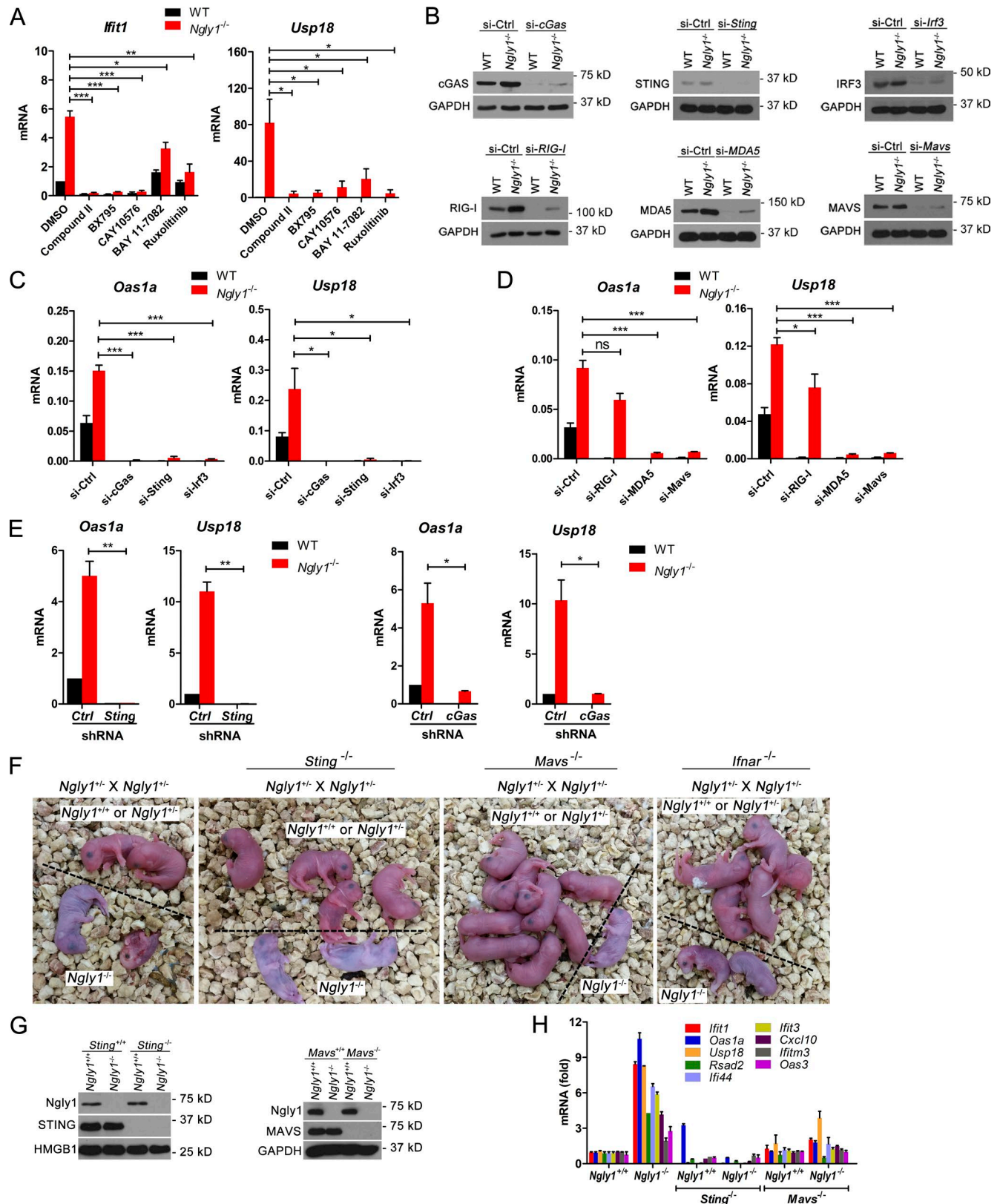


Figure 2. **Innate immune nucleic acid-sensing pathways are activated in NGLY1-deficient cells.** (A) Quantitative RT-PCR of *Ifit1* and *Usp18* in WT and *Ngly1*^{-/-} MEFs treated with indicated inhibitors for 6 h. Gene expression was normalized to the housekeeping gene *Gapdh* (same throughout). Data are representative of at least three independent experiments. Student's *t* test. (B) Western blot of indicated protein in WT and *Ngly1*^{-/-} MEFs transfected with corresponding siRNA for 48 h. GAPDH was used as a loading control. (C and D) Quantitative RT-PCR of *Oas1a* and *Usp18* in WT and *Ngly1*^{-/-} MEFs transfected with indicated siRNA for 48 h. Data are representative of at least three independent experiments. Student's *t* test. (E) Quantitative RT-PCR of *Oas1a* and *Usp18* in WT and *Ngly1*^{-/-} MEFs transduced with shRNA targeting *Sting* or *cGas*. Data are representative of at least two independent experiments. (F) Representative images of

in *Ngly1*^{-/-} MEFs, we stably expressed FLAG-tagged cGAS in WT or *Ngly1*^{-/-} MEFs using a retroviral vector, immunoprecipitated (IP) FLAG-cGAS, and isolated bound DNA (Fig. 3 A). We found that mtDNA were enriched in FLAG-cGAS pulldown in *Ngly1*^{-/-} MEFs compared with that in the WT cells (Fig. 3 B). FLAG-IP efficiency was similar in both cells (Fig. 3 A). We further depleted mtDNA using ethidium bromide in both WT and *Ngly1*^{-/-} cells and found that mtDNA depletion substantially decreased ISGs expression in *Ngly1*^{-/-} cells (Fig. S2, A and B). Ethidium bromide treatment alone slightly increased baseline ISG levels in WT cells. These data suggest that increased cytosolic mtDNA is responsible for cGAS–STING activation in *Ngly1*^{-/-} cells. In comparison, genomic DNA was not detectable in cGAS-IP complex, likely due to the mild detergent we used to isolate the cytosolic content for the IP (data not shown). We also did not detect any evidence of DNA damage in *Ngly1*^{-/-} MEFs, and both WT and *Ngly1*^{-/-} MEFs responded similarly to exogenous DNA damage caused by etoposide (Fig. S2 C). These data suggest that mitochondrial DNA is detected by cGAS in *Ngly1*^{-/-} MEFs.

The leakage of mtDNA into the cytosol prompted us to examine the mitochondrion in more detail. Using immunofluorescence microscopy, we found that mitochondria in *Ngly1*^{-/-} MEFs are severely fragmented compared with the tubular structure observed in WT cells (Fig. 3, C and D). Stable expression of WT *Ngly1* in *Ngly1*^{-/-} MEFs corrected fragmented mitochondria phenotype, suggesting that the defect was indeed caused by *Ngly1* deficiency (Fig. 3, E and F). *Ngly1*^{-/-} *Sting*^{-/-} and *Ngly1*^{-/-} *Mavs*^{-/-} primary MEFs, despite having reduced ISGs, exhibited similarly fragmented mitochondria compared with *Ngly1*^{-/-} MEFs, suggesting that mitochondrial damage occurs upstream of immune activation in *Ngly1*^{-/-} cells (Fig. S3, A and B). *NGLY1*-deficient patient fibroblasts also showed more fragmented mitochondria compared with the health control (Fig. 3, G and H). We next examined mitochondrial respiratory functions. The oxygen consumption rate (OCR), which is an indicator of mitochondrial respiration, is decreased in both basal mitochondrial respiration and maximal respiratory capacity in *Ngly1*^{-/-} compared with WT MEFs (Fig. 3 I). Together, our data suggest that *NGLY1* deficiency causes mitochondrial fragmentation, leading to impaired mitochondrial function and leakage of mtDNA and possibly RNA into the cytosol, which activate innate immune signaling.

***NGLY1* deficiency impairs mitophagy**

The mitochondrion is a dynamic organelle, and fragmented mitochondria can be caused by defects in either mitochondrial fusion or mitophagy, the latter of which is required for clearance of damaged mitochondria (Fig. 4 A; Seo et al., 2010). We first examined the expression of mitochondrial fusion proteins MFN1, MFN2, and OPR1, and found no difference between WT and *Ngly1*^{-/-} cells (Fig. S4 A). We also stressed *Ngly1*^{-/-} cells with cycloheximide or actinomycin D, both of which induce hyperfusion of mitochondria (Tondera et al., 2009). Both treatments

induced elongated tubular mitochondria in *Ngly1*^{-/-} cells, suggesting that mitochondrial fusion machinery is intact in *Ngly1*^{-/-} cells (Fig. S4 B).

We next examined the effect of *Ngly1*^{-/-} deficiency on mitophagy. We used HeLa cells stably expressing E3 ligase Parkin (HeLa/Parkin cells) to analyze mitophagy-mediated clearance of damaged mitochondria (Wei et al., 2017). We knocked down *NGLY1* expression with three different siRNAs and treated control and *NGLY1*-knockdown HeLa/Parkin cells with a combination of oligomycin and antimycin (OA) that activates mitophagy by inducing mitochondria damage (Fig. 4 B). While control siRNA-treated cells cleared damaged mitochondria effectively (note the clearance of cytoplasmic mitochondrial signal), *NGLY1* knockdown led to significantly impaired mitophagy as measured by both mtDNA (Fig. 4, C and D) and HSP60 (Fig. 4, E and F) staining. Similarly, we observed impaired mitophagy in *NGLY1*^{KO} THP-1 cells (Fig. 4, G and H). We further analyzed expression of mitophagy-related genes, and found a global decrease in expression in *Ngly1*^{-/-} MEFs compared with WT cells regardless of mitophagy inducers treatment (Fig. 4 I). Collectively, these results demonstrate that *NGLY1* deficiency impairs mitophagy leading to accumulation of damaged mitochondria. The change in mitophagy-related gene expression profile in *Ngly1*^{-/-} cells raises the possibility that *NGLY1* regulates mitochondrial homeostasis through a transcription factor.

***NGLY1* regulates mitochondrial homeostasis through transcription factor Nrf1**

Recent studies in both mammalian and *Drosophila melanogaster* cells revealed that the ER-anchored transcription factor Nrf1 requires deglycosylation by *NGLY1* in the cytosol before translocation into the nucleus and activation of proteasome genes in response to proteotoxic stress (Tomlin et al., 2017; Owings et al., 2018). Nrf1 has not been implicated in mitochondrial homeostasis, but its homologue Nrf2, which binds to similar proteasome gene targets, does play a role in autophagy and mitophagy (Digaleh et al., 2013). Nrf2 is not glycosylated and does not require *NGLY1* for its function. We thus hypothesized that Nrf1 regulates mitophagy through a transcriptional program, and that *NGLY1* deficiency causes cytosolic retention of Nrf1 due to misprocessing, which then leads to impaired mitophagy.

Nrf1 is usually undetectable at steady-state due to continuous degradation by the proteasome. After proteasome inhibitor bortezomib treatment, processed Nrf1 was observed in WT but not *Ngly1*^{-/-} cells (Fig. 5 A). Expression of proteasome subunit genes was decreased in *Ngly1*^{-/-} compared with WT cells (Fig. 5 B). After bortezomib treatment, proteasome subunit gene expression increased in WT but not *Ngly1*^{-/-} cells, consistent with *Ngly1*^{-/-} cells lacking functional Nrf1 (“processed”) and proteasome “bounce-back” response (Fig. 5 B).

Since global deletion of *Ngly1* is embryonic lethal, we generated loxP-flanked *Ngly1*^{fl/fl} mice and bred to *LysM*-Cre to generate

neonates on indicated genetic breeding backgrounds. (G) Western blot analysis of STING, MAVS, and *Ngly1* in primary MEFs of indicated genetic backgrounds. (H) Quantitative RT-PCR analysis of indicated ISGs mRNA expression in primary MEFs of indicated genetic backgrounds. Data are representative of at least three independent experiments. Error bars, SEM. *, *P* < 0.05; **, *P* < 0.01; ***, *P* < 0.001; ns indicates not significant.

Table 1. Genetic crosses of *Ngly1* mice

Background	<i>Ngly1</i> ^{-/-}			<i>Ngly1</i> ^{-/-} <i>Sting</i> ^{-/-}			<i>Ngly1</i> ^{-/-} <i>Mavs</i> ^{-/-}			<i>Ngly1</i> ^{-/-} <i>Ifnar</i> ^{-/-}		
	Neonate	Total	Live	Dead	Total	Live	Dead	Total	Live	Dead	Total	Live
<i>Ngly1</i> ^{+/+}	32.6% (77)	29.6% (70)	3.0% (7)	33.6% (177)	33.4% (176)	0.2% (1)	33.2% (75)	31.9% (72)	1.3% (3)	37.3% (50)	36.6% (49)	0.7% (1)
<i>Ngly1</i> ^{+/-}	59.7% (141)	57.6% (136)	2.1% (5)	57.6% (304)	54.6% (288)	3.0% (16)	62.8% (142)	58.8% (133)	4.0% (9)	56.0% (75)	54.5% (73)	1.5% (2)
<i>Ngly1</i> ^{-/-}	7.7% (18)	1.3% (3)	6.4% (15)	8.8% (46)	0.4% (2)	8.4% (44)	4.0% (9)	0.9% (2)	3.1% (7)	6.7% (9)	0% (0)	6.7% (9)

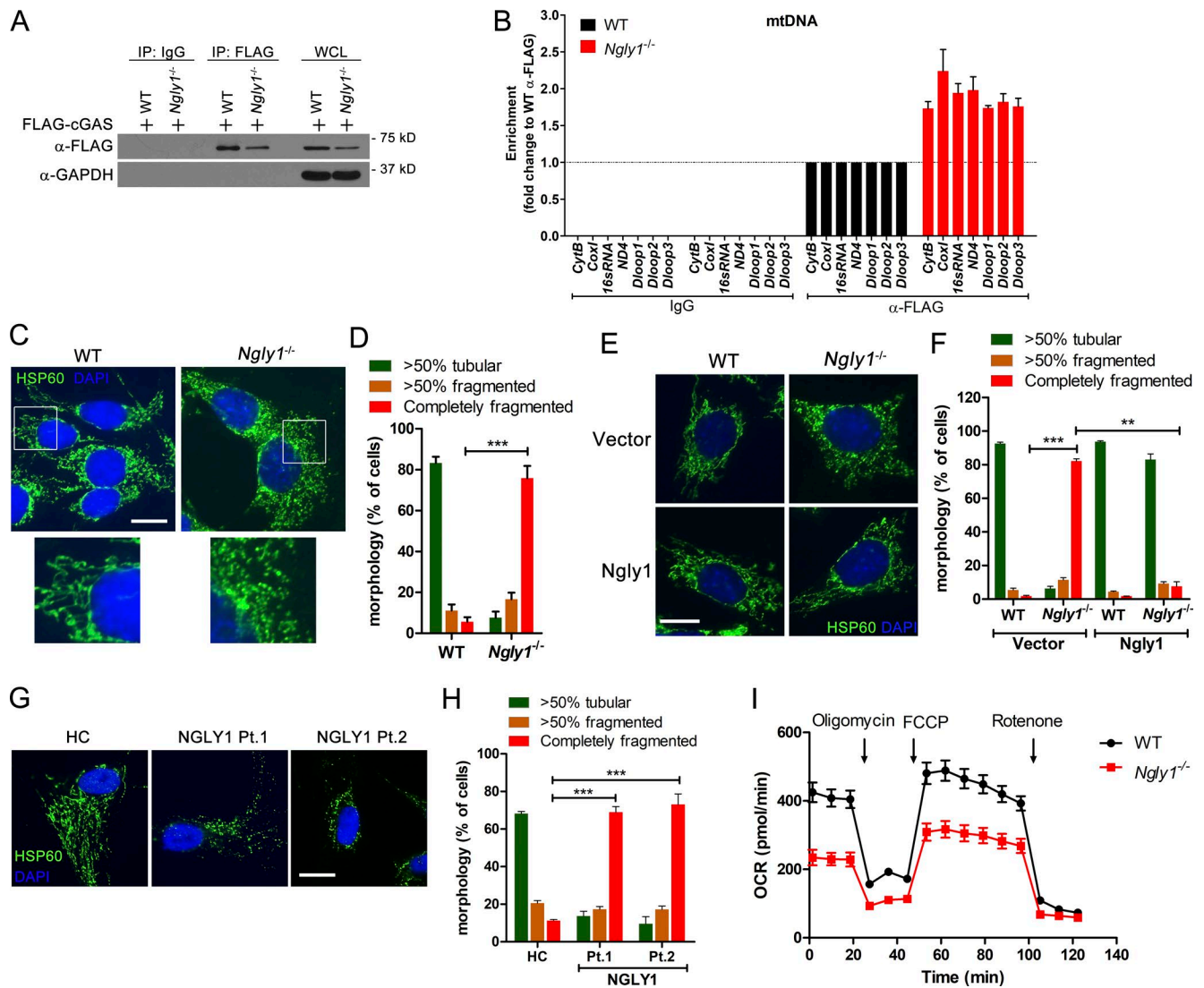


Figure 3. **NGLY1-deficient cells exhibit fragmented mitochondria and mtDNA release into the cytosol.** (A) IP of ectopically expressed FLAG-cGAS in WT and *Ngly1*^{-/-} MEFs. (B) Quantitative PCR analysis of mtDNA in FLAG-cGAS IP of WT and *Ngly1*^{-/-} MEFs. Enrichment of mitochondrial genes in *Ngly1*^{-/-} MEFs was calculated as compared with that in anti-FLAG IP of WT cells (set as 1) and normalized to FLAG-cGAS protein level shown in A. Error bars, SEM. Data are representative of three independent experiments. (C and D) Representative immunofluorescence images of HSP60 (mitochondrial marker; C) and quantitation of mitochondrial morphology (D) in WT and *Ngly1*^{-/-} MEFs. Scale bar, 10 μ m. ≥ 120 cells were enumerated for quantitation. Data were shown as mean \pm SEM of three independent experiments. Student's *t* test. (E and F) Representative images of HSP60 immunofluorescence staining (E) and quantitation of mitochondrial morphology (F) in WT and *Ngly1*^{-/-} MEFs retrovirally transduced with *Ngly1* or empty vector. Data were shown as mean \pm SEM of three independent experiments. Student's *t* test. (G and H) Representative images of HSP60 immunofluorescence staining (G) and quantitation of mitochondrial morphology (H) in human fibroblast from healthy control and NGLY1 patients. Data were shown as mean \pm SEM of three independent experiments. ****P* < 0.001 by Student's *t* test. (I) Real-time changes in the OCR of WT and *Ngly1*^{-/-} MEFs during subsequent sequential treatment with oligomycin (inhibitor of ATP synthase), FCCP (carbonyl cyanide 4-(trifluoromethoxy) phenylhydrazine), and rotenone (inhibitors of the electron-transport chain). Error bars, SEM. Data are representative of at least two independent experiments. *, *P* < 0.05; **, *P* < 0.01; ***, *P* < 0.001. Bars, 10 μ m.

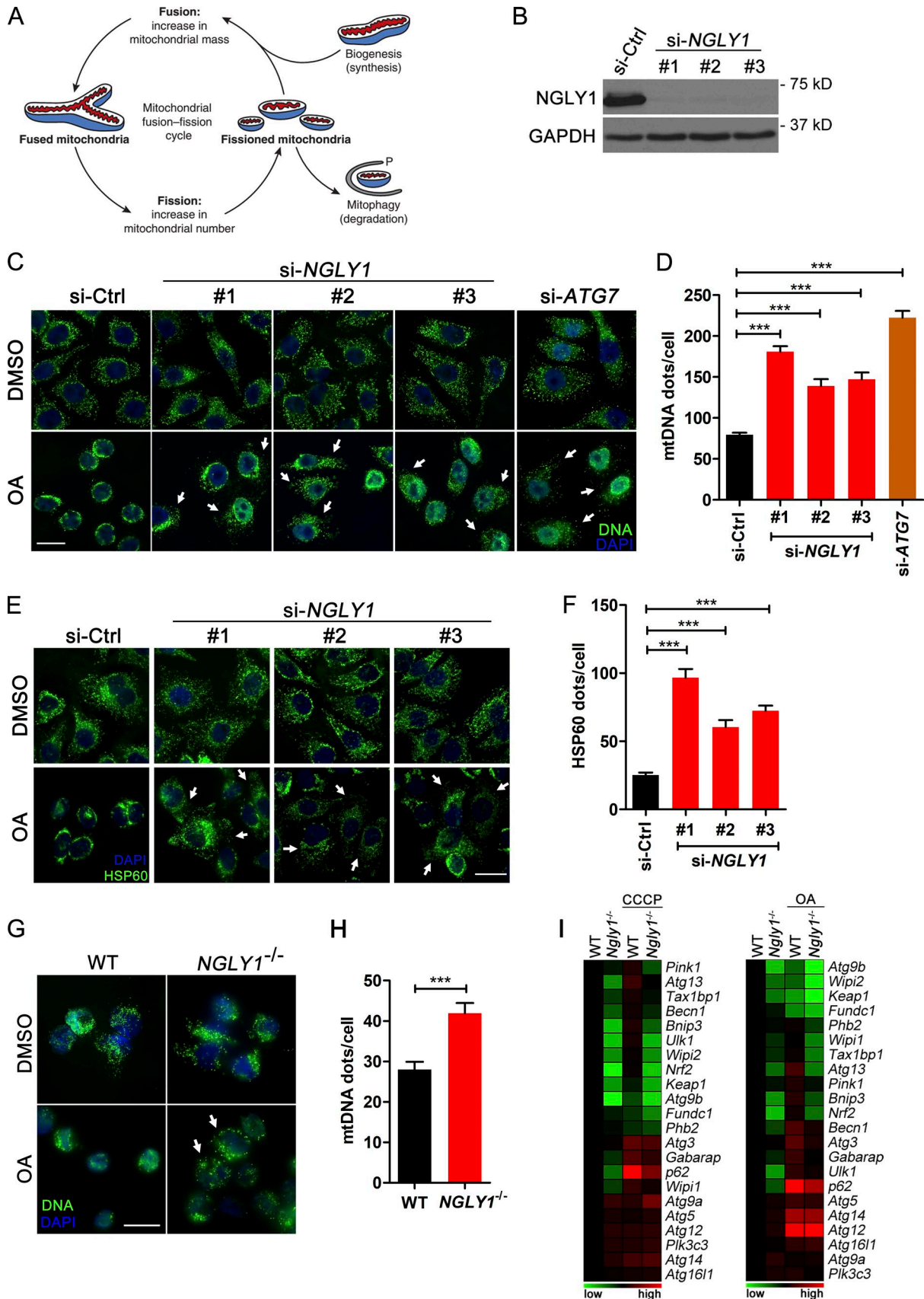


Figure 4. Impaired mitophagy in NGLY1-deficient cells. (A) Schematic diagram of mitochondrial dynamics and mitophagy. (B) Western blot analysis of NGLY1 in HeLa/Parkin cells transfected with indicated siRNA. (C) Representative images of DNA immunofluorescence staining of HeLa/Parkin cells transfected with indicated siRNA followed by either DMSO or OA (oligomycin, 2.5 μM plus antimycin, 250 nM) treatment for 16 h. White arrows denote cells with remaining

myeloid-specific *Ngly1*-deficient mice. *Ngly1^{fl/fl}LysM-Cre* mice appear healthy, with oldest ones approaching 3 mo of age. *Ngly1* protein in *Ngly1^{fl/fl}LysM-Cre* bone marrow-derived macrophages (BMDMs) was markedly reduced compared with littermate *Ngly1^{fl/fl}* (Fig. 5 C). Similar to *Ngly1^{-/-}* MEFs, *Ngly1^{fl/fl}LysM-Cre* BMDMs also showed reduced amount of processed Nrf1 after bortezomib treatment (Fig. 5 D). *Ngly1^{fl/fl}LysM-Cre* BMDMs showed a global decrease in mitophagy-related genes (Fig. 5 E) and proteasome subunit genes (Fig. 5 F). *Ngly1* processing of Nrf1 is critical for cell to withstand proteotoxic stress (Tomlin et al., 2017). We treated *Ngly1^{fl/fl}* and *Ngly1^{fl/fl}LysM-Cre* BMDMs with increasing amount of proteasome inhibitor bortezomib or carfilzomib to induce proteotoxic stress, and we found that *Ngly1^{fl/fl}LysM-Cre* BMDMs are more susceptible to cell death (Fig. 5 G). These data suggest that *Ngly1* regulates transcriptional programs of proteasome and mitophagy through Nrf1 in vitro and ex vivo. We also measured ISG expression in primary peritoneal macrophages from *Ngly1^{fl/fl}LysM-Cre* mice, and we found that expressions of several ISGs were significantly increased in *Ngly1* knockout primary peritoneal macrophages (Fig. 5, H and I).

To further test the role of Nrf1 in mitophagy defect in *Ngly1^{-/-}* cells, we stably expressed full-length or N-terminus-deleted Nrf1 (Nrf1-ΔN; Fig. 6 A), the latter of which lacks ER-anchoring sequence and mimics the cleaved and transcriptionally active fragment (Widenmaier et al., 2017). Western blot analysis showed reduced processing of ectopically expressed Nrf1 in *Ngly1^{-/-}* cells compared with WT cells and no difference for Nrf1-ΔN (Fig. 6 B), suggesting that Nrf1-ΔN is no longer regulated by NGLY1. Endogenous Nrf1 was undetectable by immunofluorescence microscopy in untreated cells. After bortezomib treatment, in vector-transduced cells, endogenous Nrf1 accumulated in the nucleus of WT cells while a substantial amount of Nrf1 remained in the cytosol in *Ngly1^{-/-}* cells (Fig. 6 C). Stable expression of full-length Nrf1 increased nuclear presence of Nrf1 in WT cells and to a lesser extent in *Ngly1^{-/-}* cells. Nrf1-ΔN was readily detectable in the nucleus of both WT and *Ngly1^{-/-}* cells even in the absence of bortezomib treatment (Fig. 6 C). Similar to the extent of nuclear localization, Nrf1 expression increased proteasome subunit gene expression in *Ngly1^{-/-}* cells, although the extent of rescue is less potent compared with Nrf1-ΔN (Fig. 6 D). We further examined mitophagy-related gene expression, and found that Nrf1 or Nrf1-ΔN expression restored many mitophagy-related gene expression in *Ngly1^{-/-}* cells with Nrf1-ΔN being more potent than full-length Nrf1 (Fig. 6, E and F). Mitochondria fragmentation phenotype of *Ngly1^{-/-}* cells was also partially rescued by Nrf1 or Nrf1-ΔN expression (Fig. 6, G and H). Moreover, elevated ISGs were also decreased in Nrf1 or Nrf1-ΔN-expressing *Ngly1^{-/-}* cells

(Fig. 6, I and J). Collectively, these data suggest that NGLY1 regulates mitochondrial homeostasis through transcription factor Nrf1. Our data also suggest that boosting nuclear activity of Nrf1 by using a transcriptionally active fragment Nrf1-ΔN can overcome the lack of NGLY1 activity and rescue both mitochondria and immune defects of *Ngly1^{-/-}* cells.

Boosting Nrf2 activity promotes mitophagy and ameliorates mitochondrial defects in *Ngly1^{-/-}* cells

Both Nrf1 and Nrf2 bind to similar cis-regulatory anti-oxidant response element (ARE) and transcriptionally activate expression of proteasome subunit gene targets. However, these two transcription factors differ in response cues and protein processing. Nrf1 responds to proteotoxic stress, while Nrf2 responds to oxidative stress. Nrf1 resides on the ER and requires deglycosylation and cleavage for activation, while Nrf2 resides in the cytosol and does not require NGLY1-mediated deglycosylation to become active (Kensler et al., 2007). Under normal condition, Nrf2 binds to cysteine-rich Keap1, which mediates ubiquitination and degradation of Nrf2. Pharmacological compounds (e.g., Keap1 inhibitors, also known as Nrf2 inducers) have been identified to disrupt that interaction to enhance Nrf2 activity. Therefore, we next explored whether we can exploit Nrf2 biology and harness existing Nrf2 inducing compounds for rescue of *Ngly1^{-/-}* cells. We first stably expressed Nrf2 in either WT or *Ngly1^{-/-}* cells. Nrf2 protein accumulated at similar levels in both WT or *Ngly1^{-/-}* cells at steady-state, and both increased to similar levels after bortezomib treatment (Fig. 7 A). Enhanced Nrf2 expression also led to exclusive nuclear localization in both WT and *Ngly1^{-/-}* cells (Fig. 7 B). *Ngly1^{-/-}* cells transduced with Nrf2 showed increased expression of mitophagy-related genes (Fig. 7, C and D), reduced mitochondrial fragmentation (Fig. 7, E and F), and decreased expression of ISGs (Fig. 7 G). Enhanced Nrf2 expression as well as Nrf1-ΔN expression also reduced cGAS-bound mtDNA in *Ngly1^{-/-}* cells (Fig. S5, A and B). These data indicate that enhancing Nrf2 expression can bypass the need for NGLY1, activate transcriptional program of mitophagy and restore mitochondrial and immune homeostasis in *Ngly1^{-/-}* cells.

Lastly, we tested whether inducing Nrf2 activity by targeting Keap1 could rescue mitochondrial defects in *Ngly1^{-/-}* cells (Fig. 8 A). Naturally derived Keap1 inhibitor sulforaphane (a natural product) robustly increased Nrf2 protein level in both WT and *Ngly1^{-/-}* cells (Fig. 8 B). Expression of proteasome subunit genes and mitophagy-related genes were broadly enhanced in *Ngly1^{-/-}* cells after sulforaphane treatment (Fig. 8, C and D). Sulforaphane treatment also markedly decreased fragmented mitochondria (Fig. 8, E and F), expression of ISGs (Fig. 8 G),

mitochondria. (D) Quantitation of cytoplasmic DNA puncta (as shown in C) in cells transfected with indicated siRNA followed by either DMSO or OA treatment. >150 cells were analyzed per condition. Data were shown as mean ± SEM of three independent experiments. Student's *t* test. (E) Representative images of HSP60 immunofluorescence staining of HeLa/Parkin cells transfected with indicated siRNA followed by either DMSO or OA treatment for 16 h. White arrows denote cells with remaining mitochondria. (F) Quantitation of cytoplasmic HSP60 puncta (as shown in E) in cells transfected with indicated siRNA followed by either DMSO or OA treatment. Data were shown as mean ± SEM of three independent experiments. Student's *t* test. (G) Representative images of immunofluorescence DNA staining of WT and *NGLY1^{-/-}* THP-1 cells treated with either DMSO or OA for 16 h. White arrows denote cells with remaining mitochondria. (H) Quantitation of cytoplasmic DNA puncta (as shown in G) in WT and *NGLY1^{-/-}* THP-1 cells treated either DMSO or OA. Data were shown as mean ± SEM of three independent experiments. Student's *t* test. (I) Heat map of autophagy and mitophagy related gene expression measured by quantitative RT-PCR in WT and *Ngly1^{-/-}* MEFs treated with either CCCP (10 μM) or OA for 8 h. ***, *P* < 0.001. Bars, 20 μm.

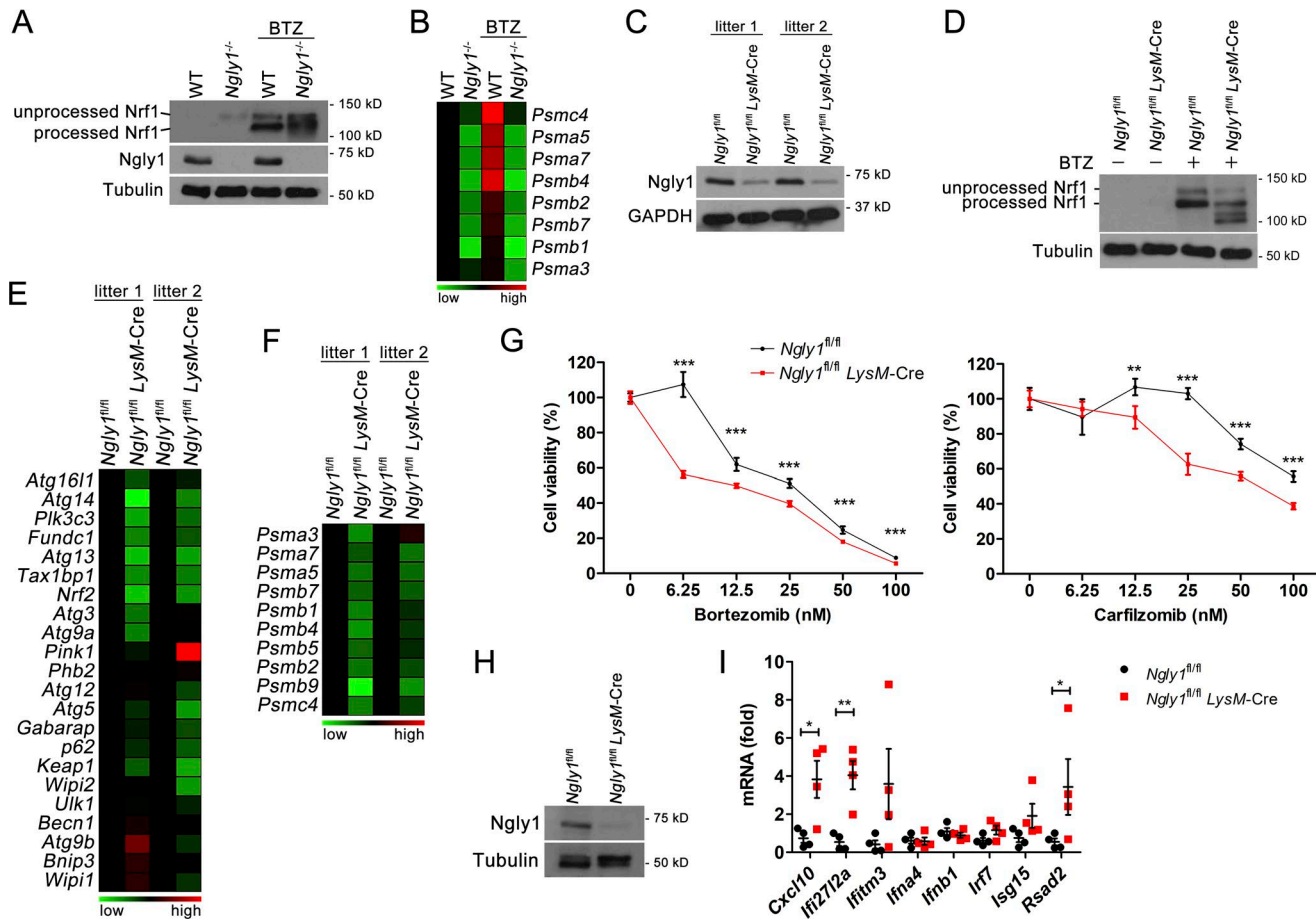


Figure 5. NGLY1 deficiency causes Nrf1 misprocessing, impairs both proteasome and mitophagy transcriptional program and activates immune signaling in mice. (A) Western blot analysis of Nrf1 in WT and *Ngly1*^{-/-} MEFs with or without proteasome inhibitor bortezomib (BTZ, 20 nM) treatment for 6 h. (B) Heat map of proteasome subunit gene expression measured by quantitative RT-PCR in WT and *Ngly1*^{-/-} MEFs with or without bortezomib (BTZ, 20 nM) treatment for 6 h. (C) Western blot of Ngly1 in BMDMs from two pairs of *Ngly1*^{fl/fl} and *Ngly1*^{fl/fl} LysM-Cre littermate mice. (D) Western blot of Nrf1 in *Ngly1*^{fl/fl} and *Ngly1*^{fl/fl} LysM-Cre BMDMs with or without Bortezomib (BTZ, 20 nM) treatment for 6 h. (E and F) Heat map of proteasome subunit genes and mitophagy-related gene expression measured by quantitative RT-PCR in BMDMs from two pairs of *Ngly1*^{fl/fl} and *Ngly1*^{fl/fl} LysM-Cre littermate mice. (G) Cell viability of *Ngly1*^{fl/fl} and *Ngly1*^{fl/fl} LysM-Cre BMDMs treated with increasing dose of proteasome inhibitor bortezomib or carfilzomib. Error bars, SEM. Student's *t* test. (H) Western blot of Ngly1 in primary peritoneal macrophages from *Ngly1*^{fl/fl} LysM-Cre and littermate *Ngly1*^{fl/fl} mice. (I) Quantitative RT-PCR analysis of ISGs in primary peritoneal macrophages from *Ngly1*^{fl/fl} LysM-Cre and littermate *Ngly1*^{fl/fl} mice (*n* = 4 mice per genotype). Error bars, SEM. Unpaired Student's *t* test. *, *P* < 0.05; **, *P* < 0.01.

and cGAS-bound mtDNA (Fig. 8 H) in *Ngly1*^{-/-} cells. These data demonstrate a novel therapeutic approach and proof-of-concept for harnessing pharmacological Nrf2 inducers to correct abnormalities of NGLY1 disease (a model in Fig. 9).

Discussion

NGLY1 deficiency is associated with a rare congenital disorder leading to global developmental delay and neurological abnormalities. The mechanism of disease is unclear and no effective therapy is available. We discovered that *NGLY1* deficiency impairs mitophagy, leading to severely fragmented mitochondria and reduced mitochondrial function. These damaged mitochondria release mtDNA and possibly also mtRNA into the cytosol, which activates cytosolic innate immune DNA- and RNA-sensing pathways, respectively, leading to chronic activation of type I IFN signaling. Depletion of mtDNA using ethidium bromide decreases ISG expressions in *Ngly1*^{-/-} cells, suggesting mtDNA

contributes to innate immune activation. Interestingly, ethidium bromide treatment also slightly increased baseline ISGs expression in WT cells likely due to other mitochondrial stresses that may indirectly activate immune signaling. The ability of mtDNA to activate the cGAS-STING DNA-sensing pathway has been largely confined to acute external stimulations so far such as inhibition of caspases (White et al., 2014) and Dengue virus infection (Aguirre et al., 2017). mtRNA and the cytosolic RNA-sensing pathways have not been analyzed carefully in these settings. In our study, we detected strong induction of ISGs in *Ngly1*^{-/-} cells and less robust but significant increase of cGAS-bound mtDNA, suggesting that other endogenous ligands beside mtDNA also contribute to innate immune signaling activation. In fact, a previous study demonstrated that mtRNA is the most potent immunostimulatory mammalian RNA type (Karikó et al., 2005). It is thus possible that impaired mitophagy and damaged mitochondria in *Ngly1*^{-/-} cells lead to leakage of both mtDNA and mtRNA into the cytoplasm that activate DNA- and RNA-sensing pathways, re-

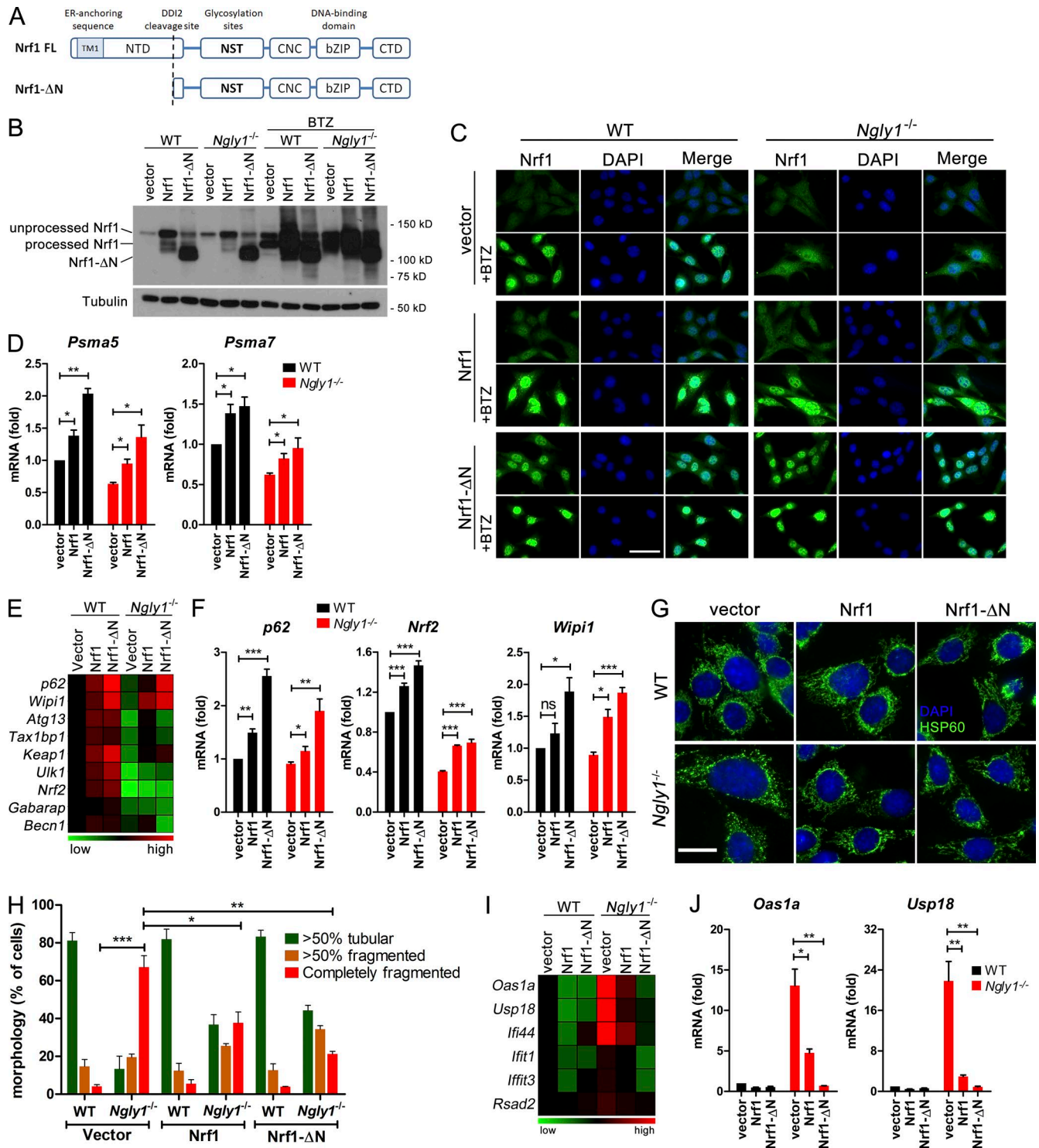


Figure 6. NGLY1 regulates mitophagy and mitochondrial homeostasis through transcription factor Nrf1. (A) Schematic diagram of full-length Nrf1 and N-terminal deleted mutant (Nrf1-ΔN). TM1, transmembrane 1. NTD, N-terminal domain. NST, Asn/Ser/Thr-rich domain. CNC, cap 'N' collar domain. bZIP, basic-leucine zipper. CTD, C-terminal domain. (B) Western blot analysis of Nrf1 in WT and *Ngly1*^{-/-} MEFs transduced with Nrf1 or Nrf1-ΔN in presence or absence of bortezomib (20 nM, 6 h). (C) Representative immunofluorescence images of Nrf1 staining of WT and *Ngly1*^{-/-} MEFs transduced with Nrf1 or Nrf1-ΔN in presence or absence of bortezomib. (D) Quantitative RT-PCR analysis of *PsmA5* and *PsmA7* in WT and *Ngly1*^{-/-} MEFs transduced with Nrf1 or Nrf1-ΔN. Data were shown as mean ± SEM of three independent experiments. (E) Heat map of mitophagy-related gene expression measured by quantitative RT-PCR in WT and *Ngly1*^{-/-} MEFs transduced with Nrf1 or Nrf1-ΔN. (F) Quantitative RT-PCR analysis of *p62*, *Nrf2*, and *Wipi1* in WT and *Ngly1*^{-/-} MEFs transduced with Nrf1 or Nrf1-ΔN. Data were shown as mean ± SEM of three independent experiments. (G and H) Representative immunofluorescence images of HSP60 (mitochondrial marker) staining (G) and quantitation of mitochondrial morphology (H) in WT and *Ngly1*^{-/-} MEFs transduced with Nrf1 or Nrf1-ΔN. Data were shown as mean ± SEM of three independent experiments. (I) Heat map of ISGs expression measured by quantitative RT-PCR in WT and *Ngly1*^{-/-} MEFs transduced with Nrf1 or Nrf1-ΔN. (J) Quantitative RT-PCR analysis of *Oas1a* and *Usp18* in WT and *Ngly1*^{-/-} MEFs transduced with Nrf1 or Nrf1-ΔN. Data were shown as mean ± SEM of three independent experiments. *, P < 0.05; **, P < 0.01; ***, P < 0.001 by Student's t test. Bars: 50 μm (C); 20 μm (G).

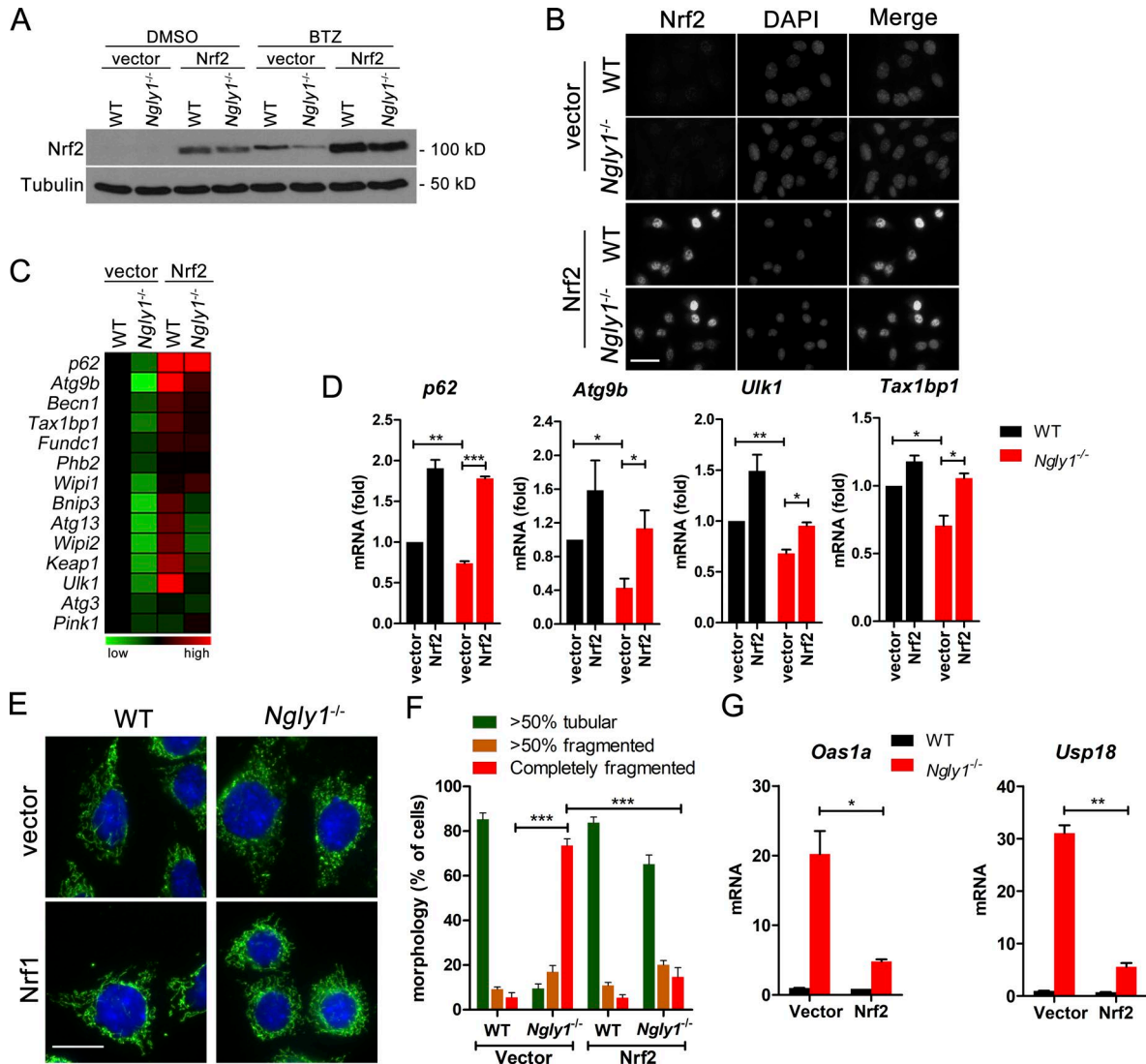


Figure 7. Enhancing Nrf2 expression activates transcriptional program of mitophagy and restores mitochondrial homeostasis in *Ngly1*^{-/-} cells. (A) Western blot analysis of Nrf2 in WT and *Ngly1*^{-/-} MEFs transduced with vector or Nrf2 in presence or absence of proteasome inhibitor Bortezomib (BTZ, 20 nM). **(B)** Representative immunofluorescence images of Nrf2 staining of WT and *Ngly1*^{-/-} MEFs transduced with vector or Nrf2. **(C)** Heat map of autophagy and mitophagy related gene expression measured by quantitative RT-PCR in WT and *Ngly1*^{-/-} MEFs transduced with vector or Nrf2. **(D)** Quantitative RT-PCR analysis of *p62*, *Atg9b*, *Ulk1*, and *Tax1bp1* in WT and *Ngly1*^{-/-} MEFs transduced with vector or Nrf2. Data were shown as mean ± SEM of three independent experiments. **(E and F)** Representative immunofluorescence images of HSP60 (mitochondrial marker) staining (E) and quantitation of mitochondrial morphology (F) in WT and *Ngly1*^{-/-} MEFs transduced with vector or Nrf2. Data were shown as mean ± SEM of three independent experiments. Student's *t* test. **(G)** Quantitative RT-PCR analysis of *Oas1a* and *Usp18* in WT and *Ngly1*^{-/-} MEFs transduced with vector or Nrf2. Data were shown as mean ± SEM of three independent experiments. *, *P* < 0.05; **, *P* < 0.01; ***, *P* < 0.001 by Student's *t* test. Bars: 50 μm (B); 20 μm (E).

spectively. Importantly, we present genetic evidence for the involvement of both DNA- and RNA-sensing pathways by breeding *Ngly1*^{-/-} mice to *Sting*^{-/-} and *Mavs*^{-/-} mice. The exact mechanism for RNA-sensing pathway activation in *Ngly1*^{-/-} cells and potential involvement of mtRNA require future investigation.

Unchecked hyperactivation of type I IFN signaling has been described in several monogenic autoimmune and autoinflammatory diseases that are collectively known as type I interferonopathies (Crow and Manel, 2015). Clinical features of type I interferonopathies are diverse, involving multiple organs depending on underlying gene mutations, although there is a striking overlap of involvement of central nervous system (CNS) and the skin (Rodero and Crow, 2016). The most severe example is

AGS (associated with mutations in nucleases *TREX1*, *RNASEH2A*, and others), which is a neuro-inflammatory disease characterized by excess IFN-α in the cerebrospinal fluid (CSF) and brain calcification detected by magnetic resonance imaging (Rodero and Crow, 2016). Increased IFN signaling in SLE is also recently reported to drive synapse loss of neurons, providing an explanation for the neurological symptoms observed in some SLE patients (Bialas et al., 2017). Abnormal brain imaging, progressive loss of neurons, and evidence of neuropathy have been reported for many NGLY1 patients (Lam et al., 2017), although NGLY1 deficiency has not been formally considered as an autoinflammatory disease. IFNs and inflammatory cytokines also have not been measured in the CSF of NGLY1 patients in limited clinical studies

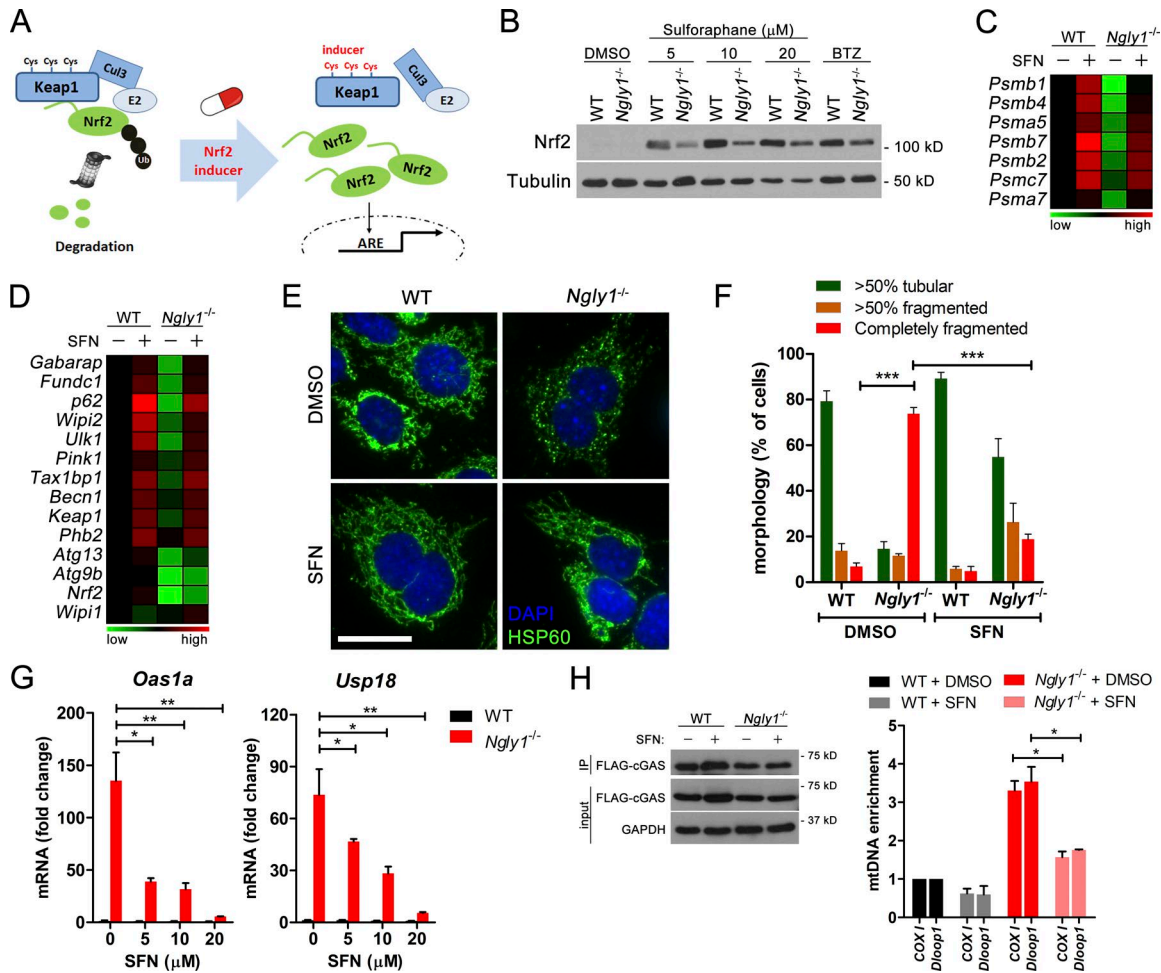


Figure 8. **Pharmacologically induction of Nrf2 promotes mitophagy and ameliorates mitochondrial defect in *Ngly1*^{-/-} cells.** (A) Schematic diagram of pharmacological activation of Nrf2 by targeting Keap1. (B) Western blot analysis of Nrf2 in WT and *Ngly1*^{-/-} treated with increasing dose of sulforaphane or proteasome inhibitor bortezomib (BTZ, 20 nM). (C and D) Heat map of proteasome subunit genes and mitophagy-related gene expression measured by quantitative RT-PCR in WT and *Ngly1*^{-/-} MEFs treated with sulforaphane (SFN, 10 μ M). (E and F) Representative immunofluorescence images of HSP60 (mitochondrial marker) staining (E) and quantitation of mitochondrial morphology (F) in WT and *Ngly1*^{-/-} MEFs treated with sulforaphane (SFN; 10 μ M) or vehicle control (DMSO). Bar, 20 μ m. Data were shown as mean \pm SEM of three independent experiments. Student's *t* test. (G) Quantitative RT-PCR analysis of *Oas1a* and *Usp18* mRNA in WT and *Ngly1*^{-/-} MEFs treated with sulforaphane (SFN) at indicated concentration. Data were shown as mean \pm SEM of three independent experiments. Student's *t* test. (H) Immunoprecipitation of ectopically expressed FLAG-cGAS (left panel) and quantitative PCR analysis of mtDNA in FLAG-cGAS IP (right panel) in WT and *Ngly1*^{-/-} MEFs treated with sulforaphane (SFN) or vehicle control (DMSO). Enrichment of mitochondrial genes in each condition was calculated as compared with that in WT cells treated with DMSO (set as 1). Data were shown as mean \pm SEM of two independent experiments. *, *P* < 0.05; **, *P* < 0.01; ***, *P* < 0.001.

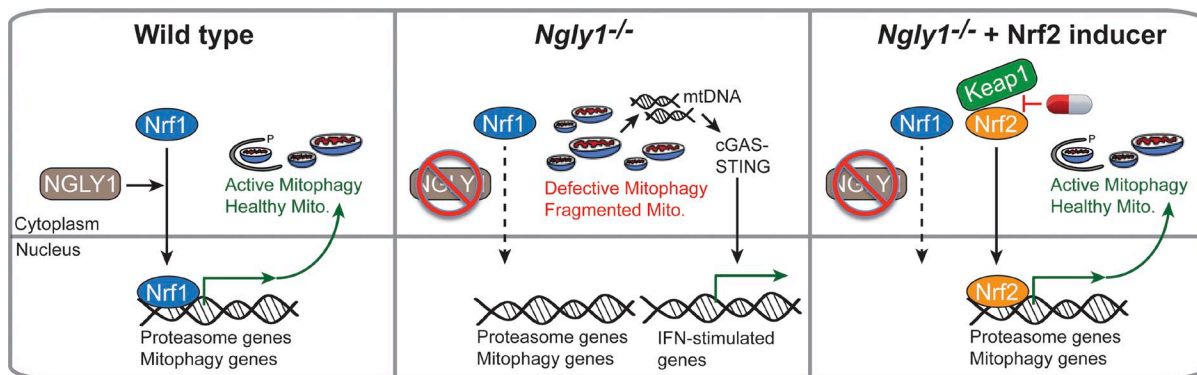


Figure 9. **A schematic model of molecular defects of *NGLY1*^{-/-} cells and potential therapeutic strategy for treating *NGLY1* disease.**

to date. However, “odd” resistance to common viral infections in *NGLY1*-deficient children has been noted by parents, and is consistent with our findings of elevated ISGs and reduced viral replication in *Ngly1*^{-/-} cells.

AGS gene deficiencies in mouse present drastically different survival phenotypes, which can be rescued to various extents after ablation of the underlying innate immune signaling pathway. For example, *Trex1*^{-/-} mice develop systemic autoinflammation due to the cGAS–STING pathway activation with an average survival of 2–3 mo; *Sting*^{-/-} fully rescues the overall survival (Gall et al., 2012; Ahn et al., 2014). In contrast, we showed that *RNASEH2A-G37S* mice also chronically activate the cGAS–STING pathway; however, these mice are still-born lethal and *Sting*^{-/-} completely eliminates the immune signaling, but only rescues 2% of the lethality (Pokatayev et al., 2016). Other functions of RNASEH2, such as maintaining genome stability, may be the main cause of lethality in mice. We found here that *Ngly1*^{-/-} mice on the C57BL/6 background is still-born lethal, chronically activates the cGAS–STING pathway, and *Sting*^{-/-} ablates the innate immune gene signature but does not rescue the overall lethality. *Ngly1*^{-/-}-mediated immune activation occurs downstream of mitochondrial defects. NGLY1 also regulates proteostasis (Tomlin et al., 2017) and mitochondrial homeostasis (this study), both of which could be important for embryonic development and survival in mice. Nonetheless, molecular immune features of the NGLY1 disease discovered here could be important for clinical features in human patients and need to be further investigated.

Our study also uncovers an unexpected connection of transcription factor Nrf1 in regulating mitophagy. Nrf1 is known for its role in regulating proteasome subunit gene expression during proteotoxic stress. Whole body *Nrf1* knockout is embryonic lethal, highlighting the importance of Nrf1 in early development. CNS-specific *Nrf1* knockout causes progressive motor neuron dysfunctions (Kobayashi et al., 2011), a clinical feature also observed in NGLY1 patients (Enns et al., 2014; Lam et al., 2017). Two recent studies using tissue-specific *Nrf1* knockouts also implicated Nrf1 in cholesterol homeostasis and brown adipose tissue thermogenic adaptation (Widenmaier et al., 2017; Bartelt et al., 2018), suggesting an expanded view of Nrf1 beyond its sole function in proteasome bounce-back response. Brown adipose tissue-specific *Nrf1* knockout causes mitochondrial damage and tissue inflammation (Bartelt et al., 2018), which remarkably mirror the immune activation and mitochondrial defects we observed in *Ngly1*^{-/-} cells and *Ngly1*-deleted myeloid tissues. Clinically, NGLY1 patients show abnormal mitochondrial physiology in muscle and liver (Kong et al., 2018). An integrated meta-transcriptome analysis of mitochondrial respiratory chain disease also identified NGLY1 as one of the most dysregulated genes (Zhang and Falk, 2014; Kong et al., 2018). NGLY1 is essential for Nrf1 deglycosylation and activation (Tomlin et al., 2017). Thus, we propose that the NGLY1–Nrf1 axis regulates proteostasis and mitochondrial homeostasis with a broad impact in inflammation, metabolism, and tissue health.

As for therapeutic strategy, we showed that ectopic expression of a transcriptionally active nuclear form of Nrf1 (that bypass the need for processing) potently rescues *Ngly1*^{-/-}-associated mitochondrial defects. Better yet, pharmacologically enhancing Nrf2

activity, which boosts expression of mitophagy-related genes, also restored mitochondrial integrity and suppressed immune activation in *Ngly1*^{-/-} cells. Although both Nrf1 and Nrf2 bind to ARE cis-regulatory element to induce target gene transcription, genetic studies show that *Nrf1*^{-/-} is embryonic lethal, while Nrf2 is dispensable for development of mice, clearly demonstrating that two transcription factors have unique target genes despite sharing overlapping ones. Nrf2 is undetectable at steady-state due to proteasome degradation mediated by E3 ligase adaptor protein Keap1, which could be the reason why Nrf2 could not compensate for lack of functional Nrf1 in *Ngly1*^{-/-} cells. Taking advantage of the Keap1–Nrf2 biology as well as existing pharmacological compounds that inhibit Keap1, we provide important proof-of-principle evidence that one such compound almost fully rescued mitochondrial and immune defects in *Ngly1*^{-/-} cells. Together, our findings not only reveal novel functions of NGLY1–Nrf1 axis in mitochondrial homeostasis and inflammation; we also demonstrate that Nrf2-enhancing drugs could have exciting potential for treating NGLY1 patients.

Material and methods

Reagents and antibodies

BX795 was purchased from Invivogen. CAY10576, BAY 11–7082, and Ruxolitinib were from Selleck Chemicals. Bortezomib and carfilzomib were from Cayman Chemical. Sulforaphane, cycloheximide, actinomycin D, oligomycin, and antimycin were obtained from Sigma-Aldrich. Mouse monoclonal *Ngly1* antibody was a gift from A. Zuberi (Jackson Laboratories). Other antibodies used as follows: anti-STING (13647; Cell Signaling; 1:1,000 dilution), phospho-STING (Ser365; D8F4W) Rabbit mAb (72971; Cell Signaling; 1:1,000 dilution), anti-cGAS (31659; Cell Signaling; 1:1,000 dilution), anti-RIG-I (3743; Cell Signaling; 1:1,000 dilution), anti-MDA5 (5321; Cell Signaling; 1:1,000 dilution), anti-tubulin (B-5-1-2; Sigma-Aldrich; 1:20,000 dilution), anti-HMGB1 (ab18256; Abcam; 1:2,000 dilution), anti-GAPDH (2118; Cell Signaling; 1:2,000 dilution), anti-SQSTM1/p62 (ab56416; Abcam; 1:1,000 dilution), anti-phosphorylated p70 S6K (Thr389; 9205; Cell Signaling; 1:1,000 dilution), anti-p70 S6K (2708; Cell Signaling; 1:1,000 dilution), anti-phospho-ATM (Ser1981) antibody (clone 10H11.E12; EMD Millipore; 1:1,000 dilution), phospho-Histone H2A.X (Ser139) antibody (2577; Cell Signaling; 1:1,000 dilution), Nrf1 (8052; Cell Signaling; 1:1,000 dilution), Nrf2 (12721; Cell Signaling; 1:1,000 dilution).

Mice

Ngly1^{-/-} C57BL/6J mice were purchased from the Jackson Laboratories (C57BL/6J-*Ngly1*^{em4Lutzj/J}, Stock No. 027060). *Sting*^{-/-} mice were obtained from G. Barber (University of Miami, Miami, FL) and *Mavs*^{-/-} mice were from Z. Chen (UT Southwestern Medical Center, Dallas, TX). *Infar*^{-/-} mice were from Taconic Biosciences. All mice were housed in specific pathogen-free animal facility of UT Southwestern Medical Center. Genotyping of *Sting*^{-/-}, *Mavs*^{-/-}, and *Infar1*^{-/-} were performed as described previously (Pokatayev et al., 2016). *Ngly1*^{-/-} mice were genotyped using Taqman probes. Primers and probes used were as follows: Fwd, 5'-TGTGTTCTGTAAGTATTCCAGGT-3'; Rev, 5'-TCTTCTTTAACC

TTGGTCCTCT-3'; WT probe, Hex-5'-TCACCTGGCGATACTCTTGTAAA-3'-Black Hole Quencher 1; *Ngly1* mutant probe, 6-FAM-5'TTGATGTACCTTGTAAACATGATG-3'-Black Hole Quencher 1. *Ngly1^{fl/fl}* C57BL/6J mice were gifts from T. Suzuki (RIKEN, Japan) and crossed with hemizygous B6.129P2-*Lyz2^{tm1(cre)If0}*/J transgenic mice (Jackson Laboratories) expressing *LysM* promoter driven Cre recombinase to generate myeloid-specific *Ngly1*-deficient mice. *Ngly1^{fl/fl}* mice were genotyped using PCR with the following primers: Fwd, 5'-GCATCACTGTCATCAGAAGCGT-3'; Rev, 5'-TGACCCACATTCAAACCTCCAGG-3'. *Ngly1^{fl/fl}**LysM*-Cre mice and *Ngly1^{fl/fl}* littermate controls were used for experiments. Animal protocol was approved by the Institutional Animal Care and Use Committee at UT Southwestern Medical Center (assurance no. APN2017-101968).

Cell culture

WT and *Ngly1^{-/-}* MEFs were gifts from Dr. T. Suzuki (RIKEN, Japan) and generated and maintained as described previously (Huang et al., 2015). *NGLY1*-deficient patient fibroblasts (GM25343 and GM25990) and lymphoid cell lines (GM25347 and GM25348) and healthy control cells were purchased from Coriell Institute. HeLa cells stably expressing Parkin (HeLa/Parkin) was generated and maintained as described previously (Sumpter et al., 2016). Primary MEFs were isolated from E13.5 embryos of indicated genetic background and maintained in DMEM supplemented with 20% FBS. BMDMs were generated as described previously (Hasan et al., 2013). Peritoneal macrophages were obtained from peritoneal cavity lavage of 6–8-wk-old *Ngly1^{fl/fl}*-*LysM*-Cre and *Ngly1^{fl/fl}* littermate control mice. All cells used in the study were tested negative for mycoplasma contamination.

Plasmids, retroviral, and lentiviral transduction

Ngly1, FLAG-tagged cGAS, FLAG-tagged Nrf1, FLAG-tagged N-terminus-deleted Nrf1 (Nrf1-ΔN), and Nrf2 were cloned into retroviral pMRX-ires-bsr vector (a gift from S. Akira) using EcoRI and NotI sites. Enzymatically inactive C306A mutant *Ngly1* was generated by site-directed mutagenesis (Agilent Technologies). Retroviruses were packaged in HEK293T cells and used for transduction followed by selection with 15 μg/ml blasticidine. For stable RNA interference, shRNA oligos were synthesized and cloned into a pLKO.1-TRC cloning vector (Addgene). Lentiviral particles were packaged in Lenti-X 293T cells following standard protocol. Cells were transduced with shRNA-harboring lentiviruses and selected with puromycin (2 μg/ml) for several days before subsequent analysis. *Ngly1* shRNA target sequences are as following: sh-*Ngly1*-1, 5'-TTAGGGTTGAAGCTCGATAT-3'; sh-*Ngly1*-2, 5'-GCTCCAATGGTTGTTGGTGAT-3'. *Sting* and *cGas* shRNA target sequences are used as reported previously (Pokatayev et al., 2016).

siRNA knockdown

Pre-designed siRNAs were purchased from Sigma-Aldrich. For transient RNA interference, cells were grown on 12-well plates and reversely transfected with 50 nM siRNA using Lipofectamine RNAiMAX Reagent per the manufacturer's instruction (Thermo Fisher Scientific). Cells were collected after 48 h and then used for quantitative RT-PCR or Western blot analysis.

CRISPR/Cas9-mediated gene targeting

To generate *NGLY1* knockout THP-1 cells by CRISPR/Cas9-mediated gene editing, guide sequences targeting *NGLY1* were designed (Zhang Lab, MIT, crispr.mit.edu [accessed April 26, 2018]) and cloned into LentiCRISPRv2 vector (Sanjana et al., 2014). The targeting guide sequences of *NGLY1* were used as following: Target 1 (T1), 5'-CTTGACGGTTCCTTGTGTGC-3'; Target 3 (T3), 5'-ACTAGACTCTTGCTGTCAG-3'. Lentiviruses carrying sgRNA and Cas9 were generated in Lenti-X 293T cells with packaging plasmids psPAX2 and an envelope plasmid pMD2.G (Addgene). THP-1 cells were transduced with lentiviruses, followed by puromycin (2 μg/ml) selection for several days. Single cell-derived clones were confirmed with Western blot for knockout of *NGLY1*.

RNA isolation and quantitative RT-PCR

Total RNA was isolated from cultured cells using TRI reagent (Sigma-Aldrich) per manufacturer's instruction, and cDNA was synthesized with iScript cDNA Synthesis kit (Bio-Rad). iTaq Universal SYBR Green Supermix (Bio-Rad) was used to quantify mRNA expression with CFX96 Real-Time PCR Detection System. Primer sequences used were described previously (Pokatayev et al., 2016) and available upon request. *Gapdh* was used as internal control to normalized gene expression. Heat map of gene expression was generated using Multiple Experiment Viewer (MeV4).

Western blot

Western blots were performed as described previously (Hasan et al., 2013). In brief, cell lysate was quantified using bicinchoninic acid assay, and equal amount of proteins were separated on SDS-polyacrylamide gel and transferred to nitrocellulose membrane. Membranes were blocked with 5% nonfat milk in 1× TBS-T and incubated with diluted primary antibodies at 4°C overnight per manufacturers' instructions. Membranes were incubated with HRP-conjugated secondary antibody (Bio-Rad) diluted for 1 h at room temperature. SuperSignal West Pico Chemiluminescent Substrate (Thermo Fisher Scientific) was used to develop the blots on film.

Immunofluorescence microscopy

Cells were grown on glass coverslips and treated as indicated. Cells were fixed with 4% paraformaldehyde, permeabilized with 0.1% Triton X-100, and blocked with 5% normal donkey serum. Slides were incubated with primary antibody for 1 h at room temperature followed by fluorescent-conjugate secondary antibody incubation, and mounted with VECTASHIELD Mounting Media containing DAPI (Vector Laboratories). Primary antibodies used were mouse monoclonal anti-HSP60 (sc-13115; Santa Cruz; 1:50 dilution), mouse anti-DNA (CBL186; Millipore; 1:25 dilution), rabbit anti-Nrf1 (8052; Cell Signaling; 1:100 dilution), and rabbit anti-Nrf2 (12721; Cell Signaling; 1:100 dilution). Secondary antibodies were donkey anti-mouse IgG Alexa Fluor 488 (A21202; Invitrogen; 1:1,000 dilution), donkey anti-rabbit IgG Alexa Fluor 488 (A21206; Invitrogen; 1:1,000 dilution), and anti-mouse IgM Alexa Fluor 488 (406522; BioLegend; 1:500 dilution). Slides were visualized with a Zeiss AxioImager Z2 microscope equipped with AxioVision software. Mitochondrial morphology was categorized and enumerated as reported (Chen et al., 2003).

Mitochondrial DNA depletion

Cells were treated with ethidium bromide (150 ng/ml; Sigma-Aldrich) for 6 d. During ethidium bromide treatment, cells were maintained in DMEM supplemented with 10% FBS, 1 mM sodium pyruvate, and 100 μ g/ml uridine. To measure mtDNA depletion efficiency, cellular DNA was isolated using QIAamp DNA mini kit, and mitochondrial *ND4* gene was quantified using real-time PCR and normalized to genomic *GAPDH* gene. The primer pair used is as following: *ND4* forward, 5'-AACGGATCCACAGCCGTA-3'; *ND4* reverse, 5'-AGTCTCGGGCCATGATT-3'. mtDNA-depleted cells were replated, cultivated overnight, and total RNA was extracted for ISGs expression measurement by real-time RT-PCR.

Mitophagy assay and automated image analysis

Mitophagy assay and automated quantification were performed as described previously (Wei et al., 2017). In brief, HeLa/Parkin cells were treated with a combination of two specific mitochondrial respiration inhibitor oligomycin (2.5 μ M) and antimycin (250 nM) for 16 h. Cells were fixed and stained with primary antibody as above. For following cell segmentation, cells were stained with CellMask Deep Red Plasma membrane stain (C10046; Invitrogen; 1:2,000 dilution) during secondary antibodies incubation. Z-stack images were acquired with Zeiss AxioImager Z2 microscope equipped with a Photometrics CoolSnap HQ2 camera using 20 \times /0.8 numerical aperture air. The same acquisition parameters were used for samples stained with identical primary antibody. Z stacks were further deconvolved with AutoDeBlur (Bitplane) before automated quantification of mitophagy using Imaris version 8.2 (Bitplane). Cell segmentation was performed based CellMask signal, and all cells touching the border of image were excluded with additional filtering. The same parameters were applied to all images within a given experiment using Imaris Batch. Data for number of cytoplasmic HSP60 or mtDNA vesicle were exported for further statistical analysis.

Quantification of cGAS-bound DNA

FLAG-cGAS IP followed by quantitative PCR was performed as described previously (White et al., 2014). In brief, WT and *Ngly1*^{-/-} MEFs were transduced or transiently transfected with a plasmid encoding FLAG-tagged cGAS. Dynabeads Protein G (10004D; Thermo Fisher Scientific) were conjugated with mouse monoclonal anti-FLAG M2 antibody (F1804; Sigma-Aldrich) or isotype mouse-IgG (I5381; Sigma-Aldrich) at 4°C overnight. Immunoprecipitation was performed following standard protocol. Before DNA extraction, a fraction of beads was eluted using loading buffer and boiled for 5 min to confirm FLAG-cGAS precipitation by Western blot. Protein G beads were treated with 200 μ g/ml protease K (Ambion) at 55°C for 30 min to release bound DNA. Co-precipitated DNA were examined by quantitative PCR and normalized to IP FLAG-cGAS. Primer sequences of mitochondrial genes are used as described previously (West et al., 2015).

Seahorse metabolism assay

For real-time analysis of the OCR, cells were seeded in Seahorse 24-well XF Cell Culture Microplates. Real-time changes in OCR were analyzed with XF-24 extracellular flux analyzer (Seahorse Bioscience) during subsequent sequential treatment with oli-

gomycin (inhibitor of ATP synthase), FCCP (carbonyl cyanide 4-(trifluoromethoxy) phenylhydrazone), and rotenone (inhibitors of the electron-transport chain) according to the manufacturer's instruction. The metabolism assay was performed at UT Southwestern Medical Center Metabolic Phenotyping Core.

Statistical analysis

Graphpad Prism was used for statistical analysis. Statistical tests performed were indicated in figure legend. Numerical data were shown as mean \pm SEM. P values of less than 0.05 were considered statistically significant.

Online supplemental material

Supplemental figures associated with this study include phosphorylation of STING (Fig. S1), mtDNA depletion and DNA damage response (Fig. S2), mitochondrial morphology in *Ngly1*^{-/-}*Sting*^{-/-} and *Ngly1*^{-/-}*Mavs*^{-/-} MEFs (Fig. S3), mitochondrial fusion (Fig. S4), and cGAS-bound mtDNA in *Ngly1*-deficient cells (Fig. S5).

Acknowledgments

We thank Aamir Zuberi (Jackson Labs) for NGLY1 antibody, Beth Levine (UT Southwestern) for mitophagy assay reagents and technical advice, Prashant Mishra (UT Southwestern) for mitochondrial fusion assay advices, and Kevin Lee and Matt Wilsey at Grace Science Foundation for communications and coordination of reagent sharing.

This work is supported by UT Southwestern Medical Center Endowed Scholar Award (N. Yan), Grace Science Foundation (N. Yan and T. Suzuki), and Mr. Hiroshi Mikitani (T. Suzuki).

The authors declare no competing financial interests.

Author contributions: N. Yan and K. Yang conceived of and designed the study. K. Yang performed most experiments and analyzed data. R. Huang assisted with mouse breeding, including crosses between *Ngly1* mice and *Sting*^{-/-}, *Mavs*^{-/-} and *Infar1*^{-/-} mice. T. Suzuki and H. Fujihira provided critical reagents and generated the *Ngly1*-flox mice. N. Yan supervised the study. N. Yan and K. Yang wrote the paper.

Submitted: 26 April 2018

Revised: 5 July 2018

Accepted: 6 August 2018

References

- Aguirre, S., P. Luthra, M.T. Sanchez-Aparicio, A.M. Maestre, J. Patel, F. Lamothé, A.C. Fredericks, S. Tripathi, T. Zhu, J. Pintado-Silva, et al. 2017. Dengue virus NS2B protein targets cGAS for degradation and prevents mitochondrial DNA sensing during infection. *Nat. Microbiol.* 2:17037. <https://doi.org/10.1038/nmicrobiol.2017.37>
- Ahn, J., P. Ruiz, and G.N. Barber. 2014. Intrinsic self-DNA triggers inflammatory disease dependent on STING. *J. Immunol.* 193:4634–4642. <https://doi.org/10.4049/jimmunol.1401337>
- Bartelt, A., S.B. Widenmaier, C. Schlein, K. Johann, R.L.S. Goncalves, K. Eguchi, A.W. Fischer, G. Parlakgöl, N.A. Snyder, T.B. Nguyen, et al. 2018. Brown adipose tissue thermogenic adaptation requires Nrfl-mediated proteasomal activity. *Nat. Med.* 24:292–303. <https://doi.org/10.1038/nm.4481>

- Bialas, A.R., J. Presumey, A. Das, C.E. van der Poel, P.H. Lapchak, L. Mesin, G. Victora, G.C. Tsokos, C. Mawrin, R. Herbst, and M.C. Carroll. 2017. Microglia-dependent synapse loss in type I interferon-mediated lupus. *Nature*. 546:539–543.
- Chen, H., S.A. Detmer, A.J. Ewald, E.E. Griffin, S.E. Fraser, and D.C. Chan. 2003. Mitofusins Mfn1 and Mfn2 coordinately regulate mitochondrial fusion and are essential for embryonic development. *J. Cell Biol.* 160:189–200. <https://doi.org/10.1083/jcb.200211046>
- Crow, Y.J., and N. Manel. 2015. Aicardi-Goutières syndrome and the type I interferonopathies. *Nat. Rev. Immunol.* 15:429–440. <https://doi.org/10.1038/nri3850>
- Digaleh, H., M. Kiaei, and F. Khodagholi. 2013. Nrf2 and Nrf1 signaling and ER stress crosstalk: implication for proteasomal degradation and autophagy. *Cell. Mol. Life Sci.* 70:4681–4694. <https://doi.org/10.1007/s00018-013-1409-y>
- East, D.A., F. Fagiani, J. Crosby, N.D. Georgakopoulos, H. Bertrand, M. Schaap, A. Fowkes, G. Wells, and M. Campanella. 2014. PMI: a $\Delta\gamma$ m independent pharmacological regulator of mitophagy. *Chem. Biol.* 21:1585–1596. <https://doi.org/10.1016/j.chembiol.2014.09.019>
- Enns, G.M., V. Shashi, M. Bainbridge, M.J. Gambello, F.R. Zahir, T. Bast, R. Crimian, K. Schoch, J. Platt, R. Cox, et al. FORGE Canada Consortium. 2014. Mutations in NGLY1 cause an inherited disorder of the endoplasmic reticulum-associated degradation pathway. *Genet. Med.* 16:751–758. <https://doi.org/10.1038/gim.2014.22>
- Fujihira, H., Y. Masahara-Negishi, M. Tamura, C. Huang, Y. Harada, S. Wakana, D. Takakura, N. Kawasaki, N. Taniguchi, G. Kondoh, et al. 2017. Lethality of mice bearing a knockout of the Ngly1-gene is partially rescued by the additional deletion of the Engase gene. *PLoS Genet.* 13:e1006696. <https://doi.org/10.1371/journal.pgen.1006696>
- Gall, A., P. Treuting, K.B. Elkon, Y.M. Loo, M. Gale Jr., G.N. Barber, and D.B. Stetson. 2012. Autoimmunity initiates in nonhematopoietic cells and progresses via lymphocytes in an interferon-dependent autoimmune disease. *Immunity*. 36:120–131. <https://doi.org/10.1016/j.immuni.2011.11.018>
- Härtlova, A., S.F. Erttmann, F.A. Raffi, A.M. Schmalz, U. Resch, S. Anugula, S. Lienenklaus, L.M. Nilsson, A. Kröger, J.A. Nilsson, et al. 2015. DNA damage primes the type I interferon system via the cytosolic DNA sensor STING to promote anti-microbial innate immunity. *Immunity*. 42:332–343. <https://doi.org/10.1016/j.immuni.2015.01.012>
- Hasan, M., J. Koch, D. Rakheja, A.K. Pattnaik, J. Brugarolas, I. Dozmorov, B. Levine, E.K. Wakeland, M.A. Lee-Kirsch, and N. Yan. 2013. Trex1 regulates lysosomal biogenesis and interferon-independent activation of antiviral genes. *Nat. Immunol.* 14:61–71. <https://doi.org/10.1038/ni.2475>
- Hasan, M., N. Dobbs, S. Khan, M.A. White, E.K. Wakeland, Q.Z. Li, and N. Yan. 2015. Cutting Edge: Inhibiting TBK1 by Compound II Ameliorates Autoimmune Disease in Mice. *J. Immunol.* 195:4573–4577. <https://doi.org/10.4049/jimmunol.1500162>
- He, P., J.E. Grotzke, B.G. Ng, M. Gunel, H. Jafar-Nejad, P. Cresswell, G.M. Enns, and H.H. Freeze. 2015. A congenital disorder of deglycosylation: Biochemical characterization of N-glycanase 1 deficiency in patient fibroblasts. *Glycobiology*. 25:836–844. <https://doi.org/10.1093/glycob/cwv024>
- Hirsch, C., D. Blom, and H.L. Ploegh. 2003. A role for N-glycanase in the cytosolic turnover of glycoproteins. *EMBO J.* 22:1036–1046. <https://doi.org/10.1093/emboj/cdg107>
- Huang, C., Y. Harada, A. Hosomi, Y. Masahara-Negishi, J. Seino, H. Fujihira, Y. Funakoshi, T. Suzuki, N. Dohmae, and T. Suzuki. 2015. Endo- β -N-acetylglucosaminidase forms N-GlcNAc protein aggregates during ER-associated degradation in Ngly1-defective cells. *Proc. Natl. Acad. Sci. USA*. 112:1398–1403. <https://doi.org/10.1073/pnas.1414593112>
- Karikó, K., M. Buckstein, H. Ni, and D. Weissman. 2005. Suppression of RNA recognition by Toll-like receptors: the impact of nucleoside modification and the evolutionary origin of RNA. *Immunity*. 23:165–175. <https://doi.org/10.1016/j.immuni.2005.06.008>
- Kensler, T.W., N. Wakabayashi, and S. Biswal. 2007. Cell survival responses to environmental stresses via the Keap1-Nrf2-ARE pathway. *Annu. Rev. Pharmacol. Toxicol.* 47:89–116. <https://doi.org/10.1146/annurev.pharmtox.46.120604.141046>
- Kobayashi, A., T. Tsukide, T. Miyasaka, T. Morita, T. Mizoroki, Y. Saito, Y. Ihara, A. Takashima, N. Noguchi, A. Fukamizu, et al. 2011. Central nervous system-specific deletion of transcription factor Nrf1 causes progressive motor neuronal dysfunction. *Genes Cells*. 16:692–703. <https://doi.org/10.1111/j.1365-2443.2011.01522.x>
- Kong, J., M. Peng, J. Ostrovsky, Y.J. Kwon, O. Oretsky, E.M. McCormick, M. He, Y. Argon, and M.J. Falk. 2018. Mitochondrial function requires NGLY1. *Mitochondrion*. 38:6–16. <https://doi.org/10.1016/j.mito.2017.07.008>
- Kwak, M.K., N. Wakabayashi, J.L. Greenlaw, M. Yamamoto, and T.W. Kensler. 2003. Antioxidants enhance mammalian proteasome expression through the Keap1-Nrf2 signaling pathway. *Mol. Cell. Biol.* 23:8786–8794. <https://doi.org/10.1128/MCB.23.23.8786-8794.2003>
- Lam, C., C. Ferreira, D. Krasnewich, C. Toro, L. Latham, W.M. Zein, T. Lehky, C. Brewer, E.H. Baker, A. Thurm, et al. 2017. Prospective phenotyping of NGLY1-CDDG, the first congenital disorder of deglycosylation. *Genet. Med.* 19:160–168. <https://doi.org/10.1038/gim.2016.75>
- Mnookin, S.2014. One of a Kind. *The New Yorker*
- Owings, K.G., J.B. Lowry, Y. Bi, M. Might, and C.Y. Chow. 2018. Transcriptome and functional analysis in a Drosophila model of NGLY1 deficiency provides insight into therapeutic approaches. *Hum. Mol. Genet.* 27:1055–1066. <https://doi.org/10.1093/hmg/ddy026>
- Pajares, M., N. Jiménez-Moreno, A.J. García-Yagüe, M. Escoll, M.L. de Ceballos, F. Van Leuven, A. Rábano, M. Yamamoto, A.I. Rojo, and A. Cuadrado. 2016. Transcription factor NFE2L2/NRF2 is a regulator of macroautophagy genes. *Autophagy*. 12:1902–1916. <https://doi.org/10.1080/15548627.2016.1208889>
- Pokatayev, V., N. Hasin, H. Chon, S.M. Cerritelli, K. Sakhuja, J.M. Ward, H.D. Morris, N. Yan, and R.J. Crouch. 2016. RNase H2 catalytic core Aicardi-Goutières syndrome-related mutant invokes cGAS-STING innate immune-sensing pathway in mice. *J. Exp. Med.* 213:329–336. <https://doi.org/10.1084/jem.20151464>
- Radhakrishnan, S.K., C.S. Lee, P. Young, A. Beskow, J.Y. Chan, and R.J. Deshaies. 2010. Transcription factor Nrf1 mediates the proteasome recovery pathway after proteasome inhibition in mammalian cells. *Mol. Cell*. 38:17–28. <https://doi.org/10.1016/j.molcel.2010.02.029>
- Rodero, M.P., and Y.J. Crow. 2016. Type I interferon-mediated monogenic autoinflammation: The type I interferonopathies, a conceptual overview. *J. Exp. Med.* 213:2527–2538. <https://doi.org/10.1084/jem.20161596>
- Rongvaux, A., R. Jackson, C.C. Harman, T. Li, A.P. West, M.R. de Zoete, Y. Wu, B. Yordy, S.A. Lakhani, C.Y. Kuan, et al. 2014. Apoptotic caspases prevent the induction of type I interferons by mitochondrial DNA. *Cell*. 159:1563–1577. <https://doi.org/10.1016/j.cell.2014.11.037>
- Sanjana, N.E., O. Shalem, and F. Zhang. 2014. Improved vectors and genome-wide libraries for CRISPR screening. *Nat. Methods*. 11:783–784. <https://doi.org/10.1038/nmeth.3047>
- Seo, A.Y., A.M. Joseph, D. Dutta, J.C. Hwang, J.P. Aris, and C. Leeuwenburgh. 2010. New insights into the role of mitochondria in aging: mitochondrial dynamics and more. *J. Cell Sci.* 123:2533–2542. <https://doi.org/10.1242/jcs.070490>
- Stetson, D.B., J.S. Ko, T. Heidmann, and R. Medzhitov. 2008. Trex1 prevents cell-intrinsic initiation of autoimmunity. *Cell*. 134:587–598. <https://doi.org/10.1016/j.cell.2008.06.032>
- Sumpter, R. Jr., S. Sirasanagandla, A.F. Fernández, Y. Wei, X. Dong, L. Franco, Z. Zou, C. Marchal, M.Y. Lee, D.W. Clapp, et al. 2016. Fanconi Anemia Proteins Function in Mitophagy and Immunity. *Cell*. 165:867–881. <https://doi.org/10.1016/j.cell.2016.04.006>
- Suzuki, T., C. Huang, and H. Fujihira. 2016. The cytoplasmic peptide: N-glycanase (NGLY1) - Structure, expression and cellular functions. *Gene*. 577:1–7. <https://doi.org/10.1016/j.gene.2015.11.021>
- Tomlin, F.M., U.I.M. Gerling-Driessen, Y.C. Liu, R.A. Flynn, J.R. Vangala, C.S. Lentz, S. Clauder-Muenster, P. Jakob, W.F. Mueller, D. Ordoñez-Rueda, et al. 2017. Inhibition of NGLY1 Inactivates the Transcription Factor Nrf1 and Potentiates Proteasome Inhibitor Cytotoxicity. *ACS Cent. Sci.* 3:1143–1155. <https://doi.org/10.1021/acscentsci.7b00224>
- Tondera, D., S. Grandemange, A. Jourdain, M. Karbowski, Y. Mattenberger, S. Herzig, S. Da Cruz, P. Clerc, I. Raschke, C. Merkwirth, et al. 2009. SLP-2 is required for stress-induced mitochondrial hyperfusion. *EMBO J.* 28:1589–1600. <https://doi.org/10.1038/emboj.2009.89>
- Wei, Y., W.C. Chiang, R. Sumpter Jr., P. Mishra, and B. Levine. 2017. Prohibitin 2 Is an Inner Mitochondrial Membrane Mitophagy Receptor. *Cell*. 168:224–238.e10. <https://doi.org/10.1016/j.cell.2016.11.042>
- West, A.P., W. Khoury-Hanold, M. Staron, M.C. Tal, C.M. Pineda, S.M. Lang, M. Bestwick, B.A. Duguay, N. Raimundo, D.A. MacDuff, et al. 2015. Mitochondrial DNA stress primes the antiviral innate immune response. *Nature*. 520:553–557. <https://doi.org/10.1038/nature14156>
- White, M.J., K. McArthur, D. Metcalf, R.M. Lane, J.C. Cambier, M.J. Herold, M.F. van Delft, S. Bedoui, G. Lessene, M.E. Ritchie, et al. 2014. Apoptotic caspases suppress mtDNA-induced STING-mediated type I IFN production. *Cell*. 159:1549–1562. <https://doi.org/10.1016/j.cell.2014.11.036>
- Widenmaier, S.B., N.A. Snyder, T.B. Nguyen, A. Arduini, G.Y. Lee, A.P. Arruda, J. Saksi, A. Bartelt, and G.S. Hotamisligil. 2017. NRF1 Is an ER Membrane Sensor that Is Central to Cholesterol Homeostasis. *Cell*. 171:1094–1109. e15. <https://doi.org/10.1016/j.cell.2017.10.003>

- Wolf, C., A. Rapp, N. Berndt, W. Staroske, M. Schuster, M. Dobrick-Mattheuer, S. Kretschmer, N. König, T. Kurth, D. Wiczorek, et al. 2016. RPA and Rad51 constitute a cell intrinsic mechanism to protect the cytosol from self DNA. *Nat. Commun.* 7:11752. <https://doi.org/10.1038/ncomms11752>
- Wu, J., and Z.J. Chen. 2014. Innate immune sensing and signaling of cytosolic nucleic acids. *Annu. Rev. Immunol.* 32:461–488. <https://doi.org/10.1146/annurev-immunol-032713-120156>
- Yan, N. 2017. Immune Diseases Associated with TREX1 and STING Dysfunction. *J. Interferon Cytokine Res.* 37:198–206. <https://doi.org/10.1089/jir.2016.0086>
- Zhang, Z., and M.J. Falk. 2014. Integrated transcriptome analysis across mitochondrial disease etiologies and tissues improves understanding of common cellular adaptations to respiratory chain dysfunction. *Int. J. Biochem. Cell Biol.* 50:106–111. <https://doi.org/10.1016/j.biocel.2014.02.012>